Low-temperature magnetic properties of marine sediments – quantifying magnetofossils, superparamagnetism, and maghemitization: eastern Mediterranean examples

Yao Qian[1], David Heslop[1], Andrew P. Roberts[1], Pengxiang Hu[1], Xiang Zhao[1], Yan Liu[2], Jinhua Li[2], Katharine M. Grant[1], and Eelco J. Rohling[1,3]

[1] Research School of Earth Sciences, Australian National University, Canberra, ACT 2601, Australia

[2] Key Laboratory of Earth and Planetary Physics, Institute of Geology and Geophysics, Chinese Academy of Sciences, Beijing 100029, P. R. China

[3] Ocean and Earth Science, University of Southampton, National Oceanography Centre, Southampton SO14 3ZH, UK

Key Points:

- Low-temperature magnetic properties of eastern Mediterranean sediments enable quantification of magnetic particle types
- Magnetofossils and superparamagnetic particles exist widely in eastern Mediterranean sediments
- Maghemitization is widespread in oxic sediment intervals and provides a measure of oxidation variations

Abstract

Periodic and marked redox changes in eastern Mediterranean marine sediments drive environmental and diagenetic changes to which magnetic minerals are sensitive. Magnetic property changes, therefore, provide useful indications of paleoceanographic conditions during and after periods of organic-rich sediment (sapropel) deposition. Magnetic properties of eastern Mediterranean sediments at room temperature have been studied for decades; however, few studies have considered low-temperature magnetic properties. Here, we investigate the low-temperature (10 to 300 K) magnetic properties of different eastern Mediterranean sediment types combined with room temperature (~300 K) magnetic properties, transmission electron microscopy, and calibrated X-ray fluorescence elemental data to illustrate the valuable information that can be obtained from low-temperature magnetic analysis of sediments. Our low-temperature magnetic results suggest that magnetite magnetofossils and superparamagnetic particles occur widely in eastern Mediterranean sediments. Superparamagnetic particle contents are highest in diagenetically reduced intervals associated with sapropels. In contrast, magnetite magnetofossils are most abundant in oxidation fronts at the tops of sapropels, where strong redox gradients formed, but are also widespread throughout other sedimentary intervals that have not been subjected to extensive reductive diagenesis. Moreover, the surfaces of magnetite particles are maghemitized (i.e. partially oxidized) in oxidation fronts at the tops of sapropels, and in other oxic sediment intervals. Our results demonstrate the value of LT magnetic measurements for quantifying diverse sedimentary magnetic signals of interest in environmental magnetism when studying paleoceanographic and paleoenvironmental processes.

1. Introduction

The semi-enclosed Mediterranean Sea is land-locked with a narrow and shallow connection to the Atlantic Ocean through the Strait of Gibraltar (Fig. 1). Due to its small volume and limited oceanic connections, Mediterranean deep-sea sediments preserve signals of climate change and a variety of interacting physical and biogeochemical processes in an amplified manner (Rohling, 1999; Rohling et al., 2014). During insolation maxima, strengthening and northward expansion of the African summer monsoon bring enhanced precipitation to North Africa, with resulting freshwater runoff into the Mediterranean Sea via both the Nile and the wider continental margin (Amies et al., 2019; Coulthard et al., 2013; Drake et al., 2013; Grant et al., 2017; Osborne et al., 2008; Rohling et al., 2002, 2004; Rossignol-Strick et al., 1982; Scrivner at al., 2004). This increased freshwater flux reduced Mediterranean surface-water salinities, increased surface productivity, inhibited deep-water ventilation, and created conditions conducive to organic-rich sediment (sapropel) formation (e.g., Castradori, 1993; Emeis et al., 2000a; 2003; Larrasoaña et al., 2003a; Myers et al., 1998; Rohling, 1994; Rohling & Gieskes, 1989; Rohling et al., 2015; Rossignol-Strick, 1983, 1985, 1987; Rossignol-Strick et al., 1982). During summer insolation minima the monsoon rain belt lay further to the south. This resulted in low freshwater flux, low Mediterranean surface water productivity, and efficient bottom-water ventilation, which favored deposition of "normal" organic-poor marls (Emeis et al., 2000b; Lourens et al., 2001; Wehausen & Brumsack, 2000).

Increased sedimentary organic matter deposition and preservation during insolation maxima and the ensuing microbial degradation produces complicated post-depositional diagenesis, which affects the magnetic properties of sapropels and sediments that underlie them (Langereis & Dekkers, 1999; Larrasoaña et al., 2003b, 2006; Liu et al., 2012; Passier et al., 2001). Anoxic sulfidic conditions during periods of sapropel deposition cause magnetic

mineral dissolution, which generally results in decreased anhysteretic remanent magnetization (ARM) values within sapropels (Fig. 2; Dekkers et al., 1994; van Santvoort et al., 1997). In addition, low ARM values may extend for tens of centimeters below sapropels when sulfate-reducing conditions were strong (Fig. 2). So-called "dissolution fronts" form in underlying marls as a result of downward diffusion of excess sulfide (Fig. 2; Larrasoaña et al., 2006; Passier et al., 2001). Conversely, increased ARM values exist commonly at the tops of sapropels as a result of iron oxide neoformation in reoxygenated bottom waters (Fig. 2; Larrasoaña et al., 2003a, 2006; Liu et al., 2012; Passier & Dekkers, 2002). This zone of elevated magnetization is referred to as the "oxidation front" (Fig. 2; Larrasoaña et al., 2003a, 2006; Liu et al., 2012; Passier et al., 2001). Based on these distinctive magnetic signatures, eastern Mediterranean sapropels can be grouped into three main types: those without oxidation fronts (type 1), those with both oxidation fronts and dissolution intervals (type 2), and those without dissolution fronts (type 3) (Larrasoaña et al., 2003b). These three sapropel types correspond to different surface productivity and bottom-water ventilation conditions (Larrasoaña et al., 2003b). Type 1 sapropels correspond to high productivity situations, while type 2 and 3 sapropels indicate moderate productivity. Bottom-waters were less well ventilated during the formation of type 1 sapropels and ventilation increased gradually when type 2 and 3 sapropels formed (Larrasoaña et al., 2003b). These three types of sapropels form under distinctive conditions, so developing a deeper understanding of their magnetic properties will aid paleoenvironmental reconstructions.

Magnetic minerals are sensitive to non-steady-state diagenesis associated with periodic accumulation and degradation of organic matter; thus, sedimentary magnetic properties can provide information concerning paleoceanographic conditions both during and after sapropel formation (Dekkers et al., 1994; Larrasoaña et al., 2003b, 2006; Roberts, 2015; Roberts et al., 1999; Robinson et al., 2000; Tarduno & Wilkinson, 1996; van Hoof et al.,

1993). Understanding the processes that influence sedimentary magnetism is, therefore, important for studying eastern Mediterranean paleoenvironments. Room temperature magnetic properties of different classes of eastern Mediterranean sediments have been studied widely (Larrasoaña et al., 2003b; Liu et al., 2012; Passier et al., 2001; Qian et al., 2020). The low-temperature (LT; 10 to 300 K) magnetic properties of eastern Mediterranean sediments are, however, less well understood (Roberts et al., 1999; Passier & Dekkers, 2002). LT properties can provide detailed information on a number of magnetic minerals. For example, the Néel temperatures of siderite and rhodochrosite at 30-40 K (Housen et al. 1996), the magnetic Besnus transition in monoclinic pyrrhotite at 34 K (Besnus & Meyer, 1964; Dekkers et al., 1989; Rochette et al., 1990, 2011), the Verwey transition in magnetite at 110-120 K (Verwey, 1939), and the Morin transition in hematite at 250-260 K (Morin, 1950) provide important mineral-specific information. In addition, LT analyses can demonstrate the occurrence of ultrafine-grained superparamagnetic (SP) particles (Banerjee et al. 1993; Smirnov & Tarduno 2000) and magnetite magnetofossils (Chang et al., 2016; Moskowitz et al. 1993; Passier & Dekkers, 2002). Moreover, LT measurements can provide information about the extent of maghemitization (partial surface oxidation of magnetite) (Chang et al., 2013; Özdemir & Dunlop, 2010; Passier & Dekkers, 2002; Smirnov & Tarduno, 2000, 2001). Passier & Dekkers (2002) analyzed the LT magnetic properties of the most recent eastern Mediterranean sapropel (S1). They proposed that SP particles and biogenic magnetite formed at the oxic-suboxic boundary, and that maghemitization occurred in the pyritized zone beneath sapropels. In contrast to S1, the LT magnetic properties of other eastern Mediterranean sediments (i.e., the three sapropels types mentioned above and intercalated marls) remain unknown.

In this study, LT magnetic analyses with hysteresis loops, first-order reversal curves (FORCs), transmission electron microscope (TEM) observations, calibrated X-ray

fluorescence (XRF) elemental data (Grant et al., 2017), and high-resolution bulk magnetic properties (Qian et al., 2020) are combined to investigate eastern Mediterranean sediments. Our results provide insights into various diagenetic effects on magnetic minerals under reducing conditions and illustrate the value of LT analyses in identifying environmental magnetic signals of interest in paleoceanographic and paleoenvironmental studies.

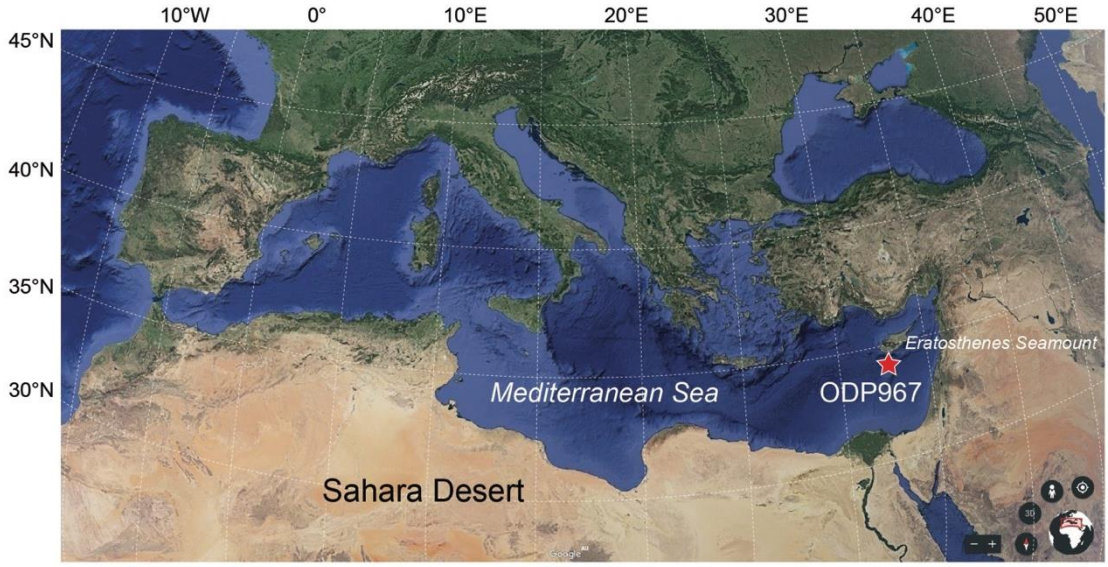

Fig. 1 Location of ODP Site 967 (34°04'N, 32°43'E, 2,553 m water depth) and Eratosthenes Seamount (map generated from Google Earth).

2. Samples

Sediments were sampled from Ocean Drilling Program (ODP) Site 967 (Fig. 1), eastern Mediterranean Sea (Shipboard Scientific Party, 1996). Core sections 5H6 to 5H7 from Hole 967C were studied here, which span approximately 2.7 m from 49.99 to 52.69 meters composite depth (mcd). These sections are dated to between 1.59 and 1.71 Ma in the age model of Grant et al. (2017). The studied sediments contain several well-developed sapropels of two main types, which provide a range of environmental conditions to assess the

usefulness of LT magnetic analyses in paleoenvironmental studies. Forty-four samples from three representative intervals were selected for LT analyses (red circles; Figs. 3 and 4), and twenty-nine samples were selected for FORC measurements (Fig. S1). Eighty-one sediment samples were selected for hysteresis measurements (black circles; Fig. 4) based on their bulk magnetic properties (Qian et al., 2020).

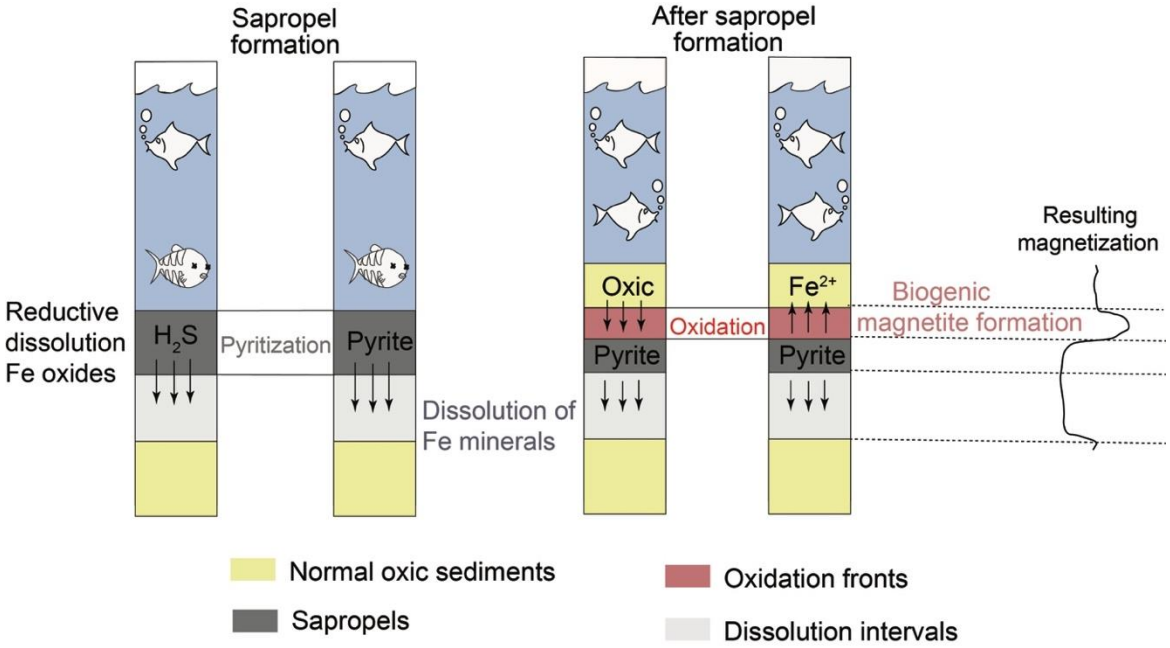

Fig. 2 Illustration of sapropel formation and magnetization (e.g., ARM) variations in the eastern Mediterranean Sea (characteristic of a Type 2 sapropel; Larrasoaña et al., 2003). Modified from Roberts (2015).

3. Methods

3.1 Magnetic measurements

All magnetic measurements were performed at the Paleomagnetism Laboratory, Australian National University (ANU). The studied samples were collected at 1-cm stratigraphic intervals and were placed into plastic cubes. A shielded narrow-access 2-G Enterprises cryogenic magnetometer was used to measure ARM and saturation isothermal

remanent magnetization (SIRM). In this study, the ARM was imparted by applying a peak alternating field (AF) of 100 mT and a direct current (DC) bias field of 0.05 mT, and the SIRM was acquired with an induction field of 900 mT. χ_{ARM}/χ, ARM/SIRM, and SIRM/χ were measured to indicate magnetic grain size variations, where χ_{ARM} (susceptibility of ARM) is calculated as ARM/DC bias field (King et al., 1982; King & Channell, 1991). The coercivity parameter, S-ratio (= 0.5 × [1-($IRM_{-0.3T}$/SIRM)]), is used to make inferences about the relative abundances of low- to high-coercivity minerals, where $IRM_{-0.3T}$ was imparted with a backfield of 0.3 T (Bloemendal et al., 1992).

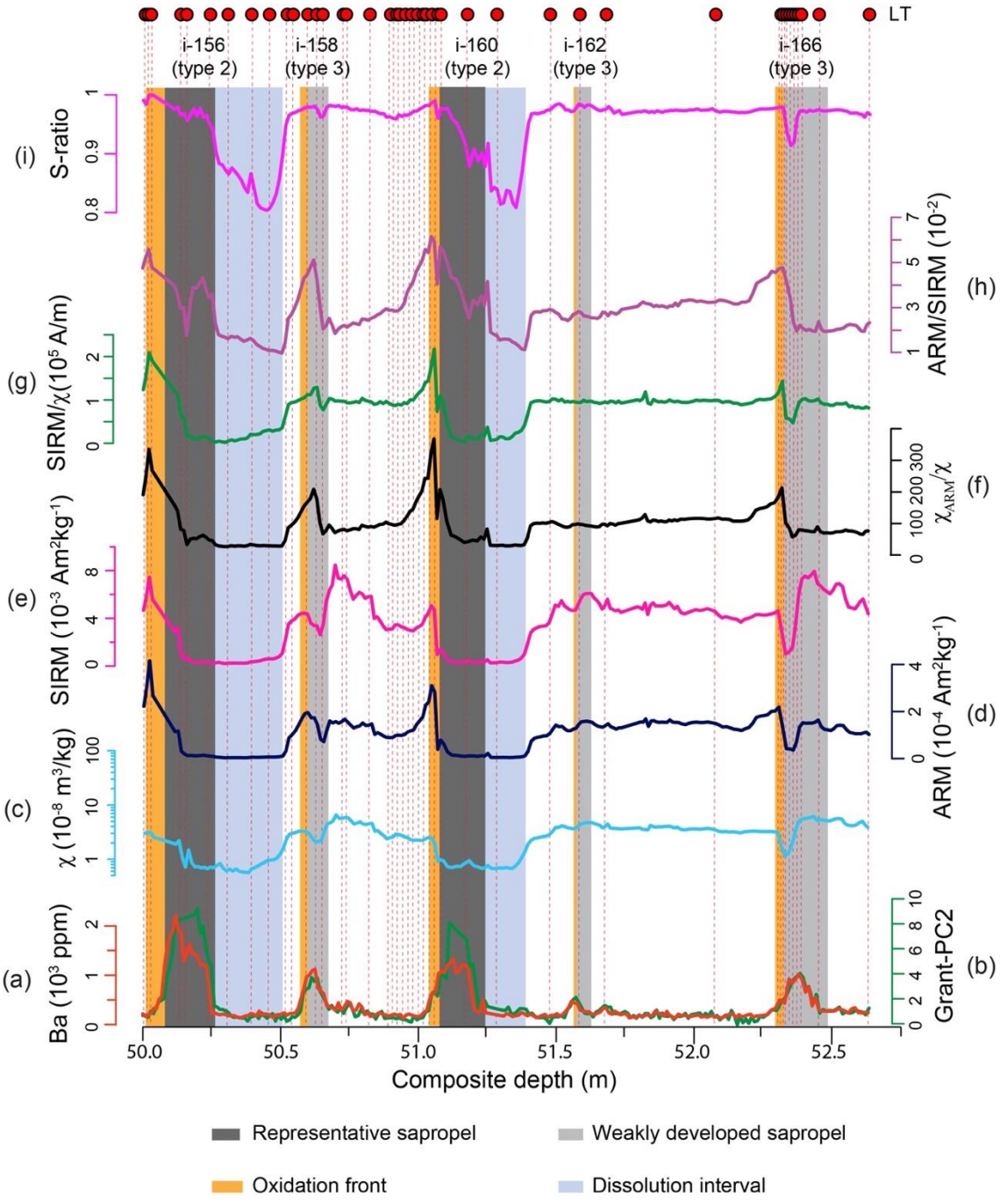

158

159 **Fig. 3** Down-core variations of geochemical data and environmental magnetic parameters.
160 Elevated (a) Ba (orange) and (b) Grant-PC2 (dark green) indicate the positions of sapropels.
161 Discrete sample data include (c) χ (cyan); (d) ARM (dark blue); (e) SIRM (pink); (f) χARM/χ
162 (black); (g) SIRM/χ (green); (h) ARM/SIRM (purple); and (i) S-ratio (magenta). Forty-four
163 samples selected for LT analyses are indicated by red circles at the top of the figure. Dark
164 gray and light gray shadings denote the locations of representative and weakly developed

sapropels, respectively. Orange and blue shadings correspond to the locations of oxidation fronts and dissolution intervals, respectively. Sapropel stratigraphy is based on Emeis et al. (2000), where the numeric number followed by "i-" is the insolation cycle. Modified from Qian et al. (2020).

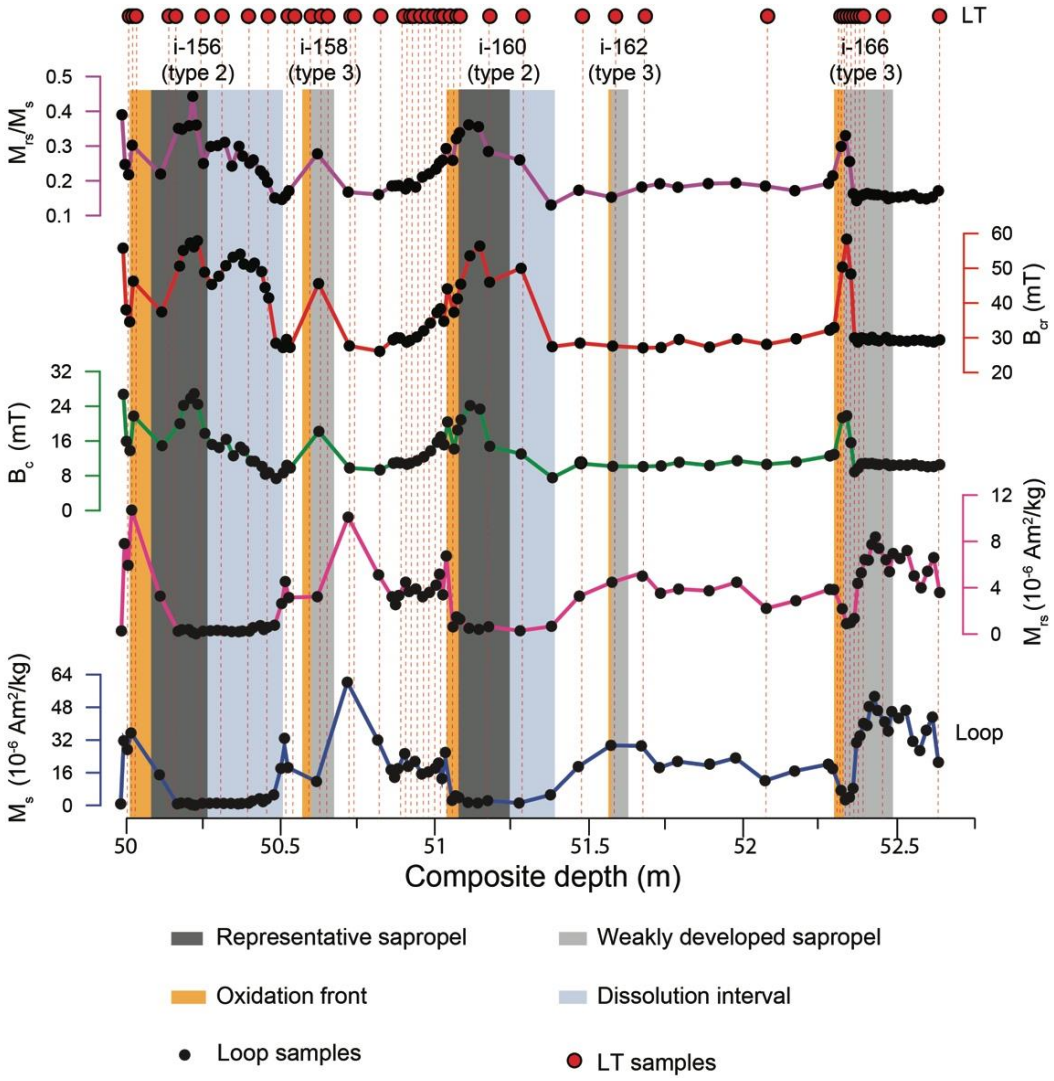

Fig. 4 Profiles of M_s, M_{rs}, B_c, B_{cr}, and M_{rs}/M_s versus depth. Red circles and the meaning of colored shadings are identical to Fig. 3.

Hysteresis loops and first-order reversal curves (FORCs; Pike et al., 1999) were measured on representative samples. Measurements were performed using a Princeton Measurements Corporation MicroMag Model 3900 vibrating sample magnetometer (VSM).

Hysteresis curves were measured to ±500 mT, with field step and averaging times of 3 mT and 500 ms, respectively. Saturation magnetization (M_s), saturation remanent magnetization (M_{rs}), and coercive force (B_c) were obtained from loops, while the coercivity of remanence (B_{cr}) was obtained from backfield demagnetization curves after applying a saturation IRM along with hysteresis loops on the same system. FORCs were measured with the irregular grid FORC protocol of Zhao et al. (2015). A 300 ms averaging time was used for weakly magnetized samples (M_{rs} < 1 μAm^2), while other samples (M_{rs} > 1 μAm^2) were measured with a 200 ms averaging time. FORC data were processed and plotted using the xFORC software with a smoothing factor of 3 or 4 based on sample noise level (Zhao et al., 2015, 2017).

A Quantum Design (QD) Magnetic Property Measurement System (MPMS; model XL7) was used for LT magnetic measurements of forty-four samples. A 5 T DC field was imparted to produce a room temperature SIRM (RTSIRM), which was then measured from 300 K to 10 K and then back to 300 K at 1 K intervals in zero field. This measurement is referred to as LT cycling (LTC) of a RTSIRM. Zero-field-cooled (ZFC) and field-cooled (FC) measurements were conducted following the method used in Qian et al. (2020). The superconducting MPMS magnet was "reset" after each field application to eliminate trapped fields. The MPMS system used here includes the QD Environmental Shield and ultra-low field option. However, small residual fields can remain after a magnet reset. Therefore, paramagnetic phases could contribute to measured LTC of RTSIRM, ZFC, and FC curves, particularly at low temperatures. We expect the remanence to dominate and this paramagnetic contribution should be minor.

3.2 TEM observations

Extraction and characterization of magnetic minerals from sediments were performed following Li et al. (2020a). TEM analysis was conducted at the Institute of Geology and

Geophysics, Chinese Academy of Sciences (IGG-CAS) using a JEM-2100HR TEM with a LaB_6 gun and 200 kV accelerating voltage.

4. Sapropel identification

Sapropels were identified based on calibrated XRF elemental data (Grant et al., 2016) and the Grant-PC2 record (Grant et al., 2017). Grant-PC2 is a principal component estimated from geochemical results of eastern Mediterranean sediments, which contain several elements associated with sapropel formation (Grant et al., 2017; Qian et al., 2020). Using these two parameters together provides a comprehensive indication of sapropel locations. High Ba concentrations and Grant-PC2 values suggest that there are five sapropels of two types within the studied sediments. These two sapropel types are "representative" sapropels, i-156 and i-160, with well-developed oxidation fronts and dissolution intervals (type 2 according to Larrasoaña et al. (2003b); dark gray shading in Figs. 3-10) and "weakly developed" sapropels, i-158, i-162, and i-166, with well-developed oxidation fronts but without dissolution intervals (type 3 according to Larrasoaña et al. (2003b); light gray shading in Figs. 3-10), respectively. Thus, the studied sediments can be divided into three main parts: (1) representative sapropels (i-156 and i-160; Figs. 3-10), (2) weakly developed sapropels (i-158, i-162, and i-166; Figs. 3-10), and (3) background marls (Figs. 3-10).

5. Room temperature magnetic properties

Room temperature magnetic properties were reported by Qian et al. (2020) for the selected sediment interval. For representative sapropels, high ARM and SIRM values are observed in oxidized sediments above sapropels, which indicates a large proportion of ferrimagnetic minerals at oxidation fronts (Fig. 3). High χ_{ARM}/χ, ARM/SIRM, and SIRM/χ values in the

oxidized sediments indicate that the ferrimagnetic minerals are more likely to be fine stable single domain (SSD)/vortex state grains (Fig. 3). However, ARM and SIRM values drop rapidly within sapropels and underlying dissolution intervals due to magnetic mineral dissolution (Fig. 3). Low χ_{ARM}/χ, ARM/SIRM, and SIRM/χ values indicate that residual magnetic minerals in these intervals are mainly coarser grains (Fig. 3). This is also evident from extremely low S-ratios in the dissolution intervals (Fig. 3), which results from preferential removal of fine-grained magnetite. In addition, except for low ARM and SIRM values in the middle of weakly developed sapropels, other sediment intervals normally have high values (Fig. 3). Grain size parameters have almost the same variations in both representative sapropels and weakly developed sapropels, with high χ_{ARM}/χ, ARM/SIRM, and SIRM/χ ratios in oxidation fronts and low values within sapropels and underlying sediments (Fig. 3). Compared to representative sapropels, the low values appear in the bottom parts of weakly developed sapropels (Fig. 3). This suggests that sulfidic dissolution is not strong in weakly developed sapropels. Furthermore, for normal sediments, all parameters remain stable. Specifically, ARM, SIRM, χ_{ARM}/χ, ARM/SIRM, and SIRM/χ change rapidly with lower values in dissolution intervals/weakly developed sapropels and higher or intermediate values between sapropels; S-ratios have relatively constant high values (Fig. 3).

6. Results

6.1 Hysteresis properties

Hysteresis parameters are expressed in mass-normalized magnetic units, which account for sediment porosity variations. M_s and M_{rs} undergo similar stratigraphic variations; both increase sharply within oxidized sapropels, where maximum values are typically observed, and then decrease to minima within dissolution fronts beneath sapropels (Fig. 4).

M_{rs}/M_s increases within oxidation fronts from 0.15 to 0.5 (Fig. 4), which is indicative of SSD magnetite formation (potentially of biogenic origin) that formed at the tops of sapropels during bottom water reoxygenation (Garming et al., 2004; Kruiver & Passier, 2001; Larrasoaña et al., 2003b, 2006; Passier et al., 2001). Within marls, B_c and M_{rs}/M_s oscillate around values of 10 mT and 0.2, respectively, which is typical of many marine sediments (Fig. 4; Garming et al., 2004; Larrasoaña et al., 2007; Passier & Dekkers, 2002; Roberts et al., 2012). In contrast, high B_c, B_{cr}, and M_{rs}/M_s values indicate that high-coercivity minerals dominate in sapropels and dissolution intervals. This is probably a result of preferential magnetite dissolution.

6.2 Low-temperature magnetic properties

6.2.1 ZFC and FC warming

ZFC and FC warming curves have stratigraphic dependencies associated with different diagenetic zones. All ZFC and FC warming curves contain large remanence drops below 50 K, possibly due to the presence of SP grains (Fig. 5). Marked remanence drops between 10 and 50 K do not appear to be associated with siderite because we observe no features that could correspond to a Néel point of 38 K (Housen et al., 1996). For representative sapropels, two distinctive inflections are observed for samples from the overlying oxidation front. These inflections are related to the Verwey transition temperature (T_v) at ~95 K and ~110 K for magnetite (Fig. 5a) due to a combination of inorganic and biogenic magnetite. The remanence loss at ~95 K, which is related to biogenic magnetite, is more pronounced than that at ~110 K due to inorganic magnetite (Chang et al., 2016). The Verwey transition is not evident in the ZFC/FC derivatives in other regions of representative sapropels (Fig. 5a), which suggests that magnetite has been destroyed by reductive dissolution (Roberts, 2015). For marl samples, all ZFC and FC curves contain a double T_v signature (Fig. 5c). FC curves

have stronger remanences than ZFC curves. However, the remanence difference across all temperatures between FC and ZFC curves, especially around the Verwey transition, is smaller in marls than in oxidation fronts. The magnitude of the double T_v feature varies with depth, likely resulting from variable partial magnetite oxidation. The double T_v signature is present in all samples from the weakly developed sapropel, although it is attenuated through the middle of the sapropel (Fig. 5b).

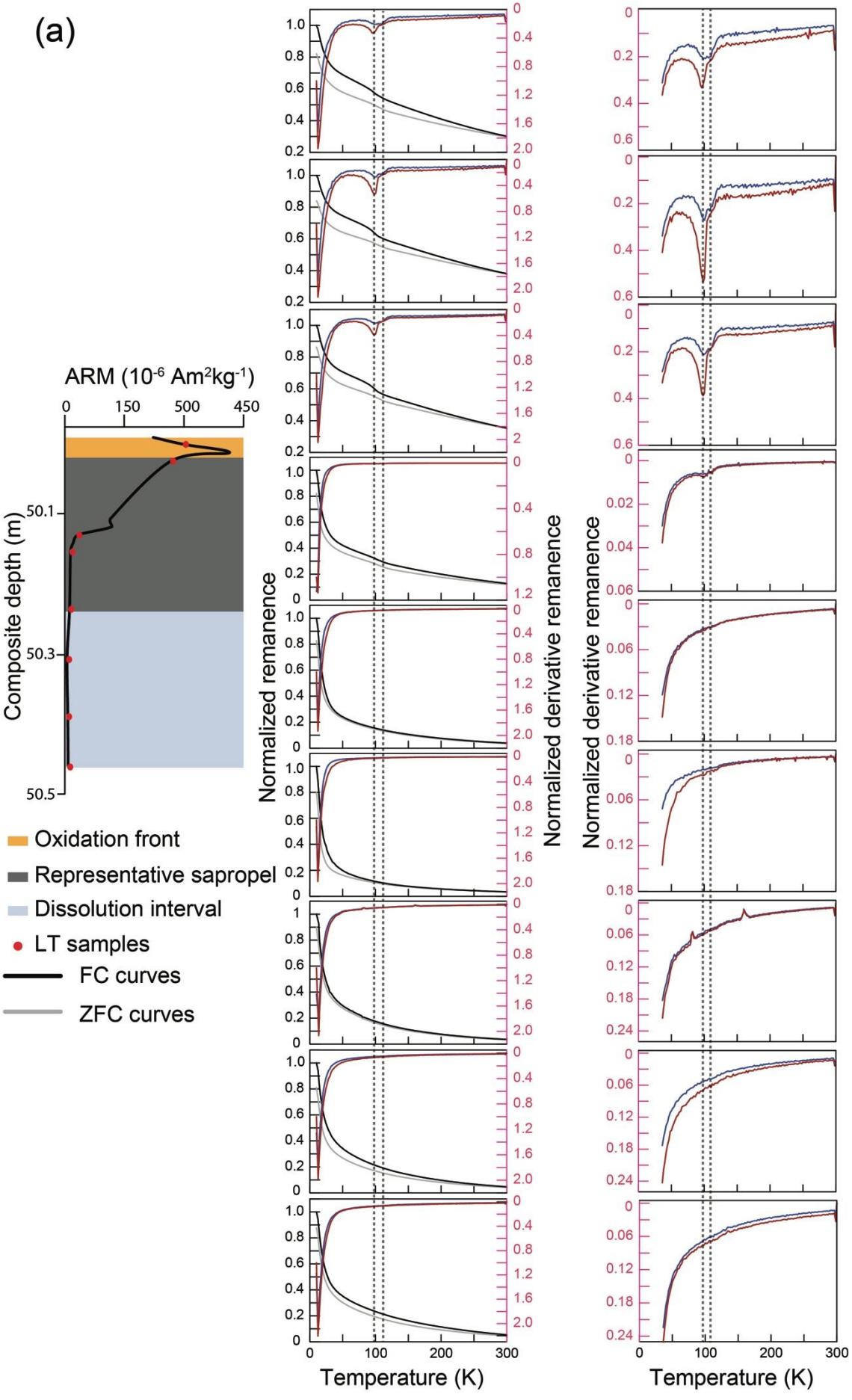
(a)
ARM (10^{-6} Am^2kg^{-1})
0
150
500
450
Composite depth (m)
50.1
50.3
50.5
Oxidation front
Representative sapropel
Dissolution interval
LT samples
FC curves
ZFC curves
Normalized remanence
Normalized derivative remanence
Normalized derivative remanence
Temperature (K)
Temperature (K)

279

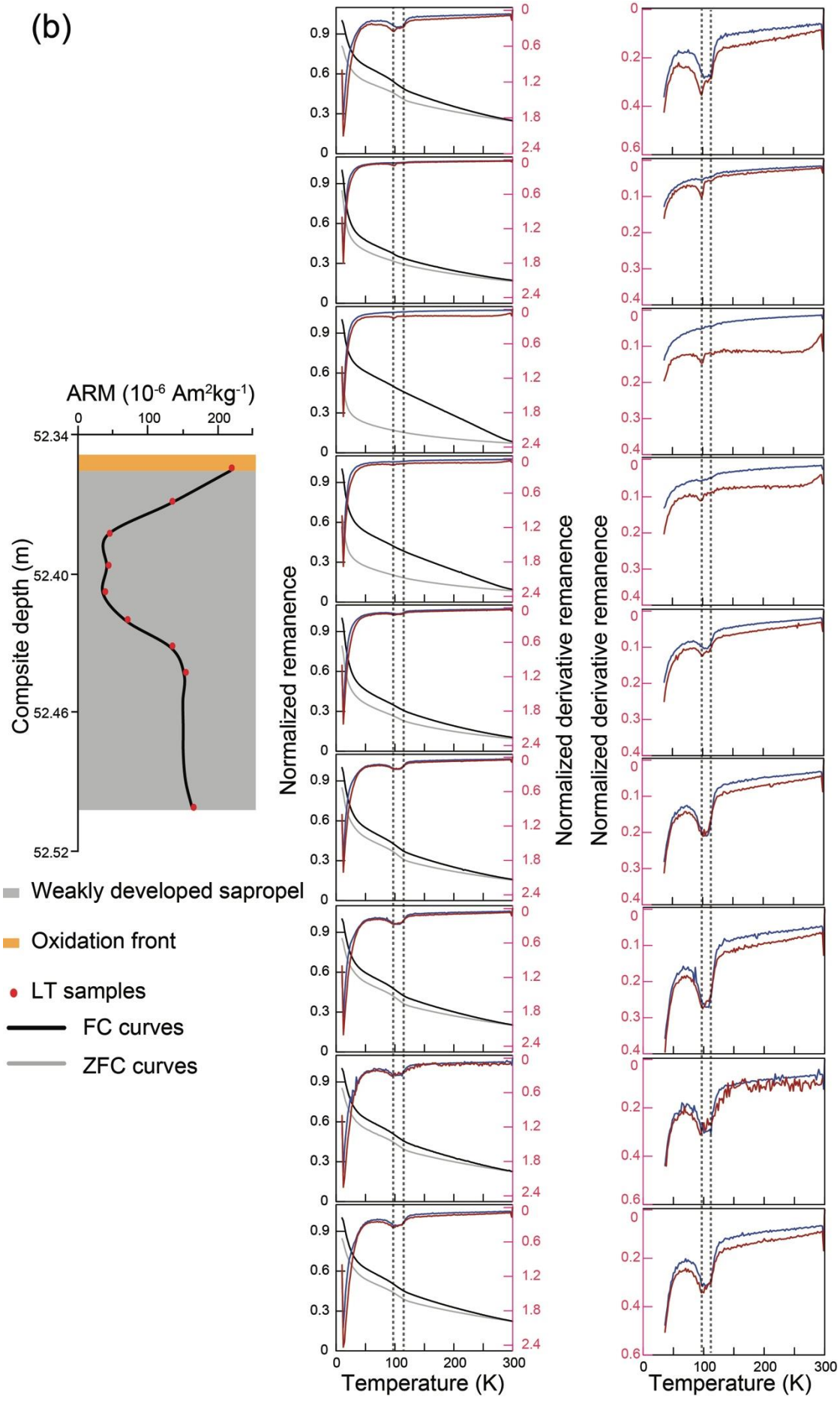
(b)
ARM (10^{-6} Am^2kg^{-1})
0
100
200
52.34
52.40
52.46
52.52
Compsite depth (m)
Weakly developed sapropel
Oxidation front
LT samples
FC curves
ZFC curves
Normalized remanence
Normalized derivative remanence
Normalized derivative remanence
0
100
200
300
Temperature (K)
Temperature (K)

280

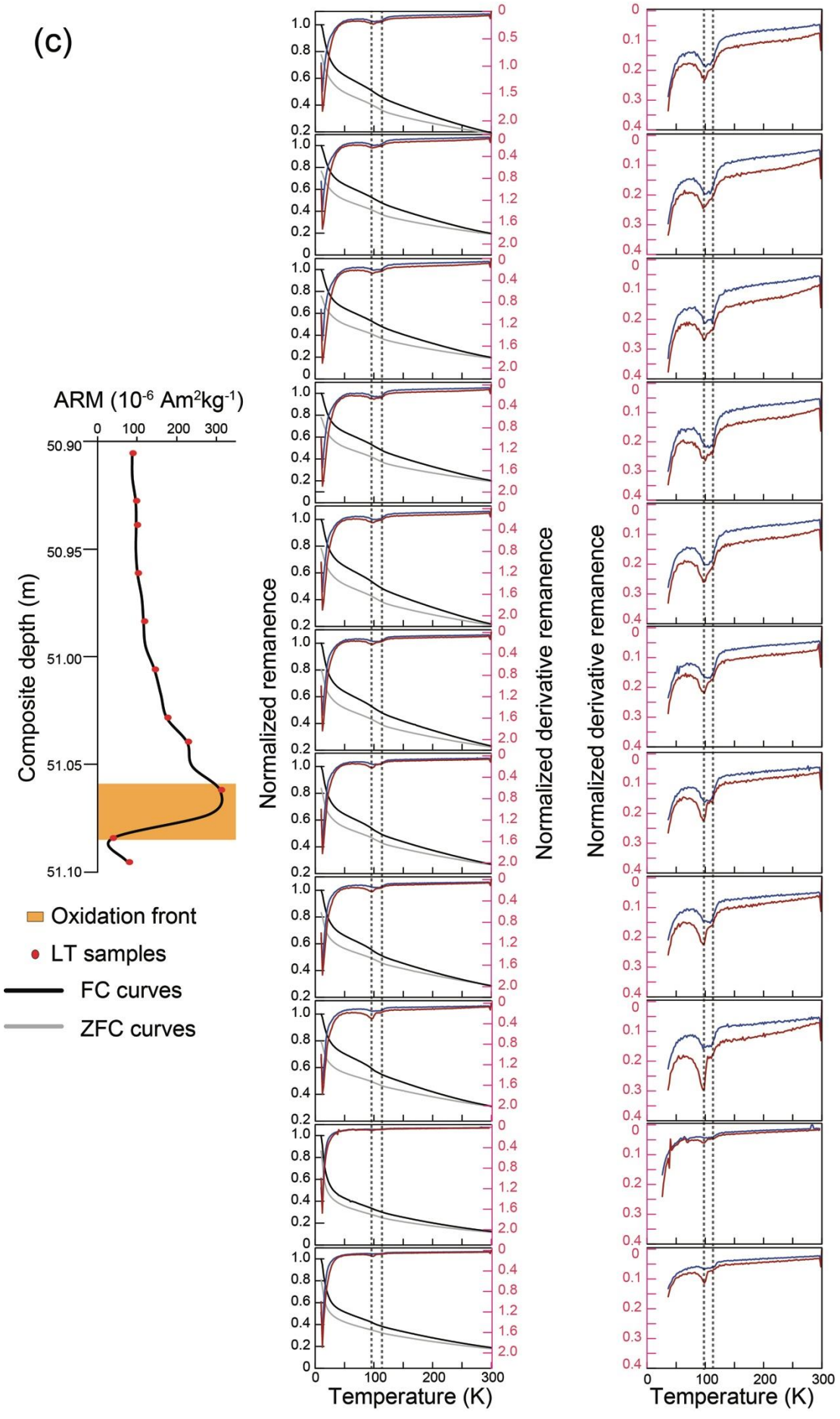
(c)
ARM (10^{-6} Am^2kg^{-1})
0
100
200
300
50.90
50.95
51.00
51.05
51.10
Composite depth (m)
Oxidation front
LT samples
FC curves
ZFC curves
Normalized remanence
Normalized derivative remanence
Normalized derivative remanence
Temperature (K)
Temperature (K)

281

Fig. 5 ZFC and FC curves for samples from representative sedimentary intervals. ARM profile with sample locations indicated by red circles selected from (a) a representative sapropel (left), ZFC (gray) and FC (black) curves and their derivatives (blue (ZFC); red (FC)) (middle) and enlarged derivative curves (right). (b) Same as (a) but for a weakly developed sapropel (left). (c) Same as (a) but for marls. Dark gray, light gray, orange, and light blue shading indicate the respective representative sapropel, weakly developed sapropel, oxidation front, and dissolution interval, respectively.

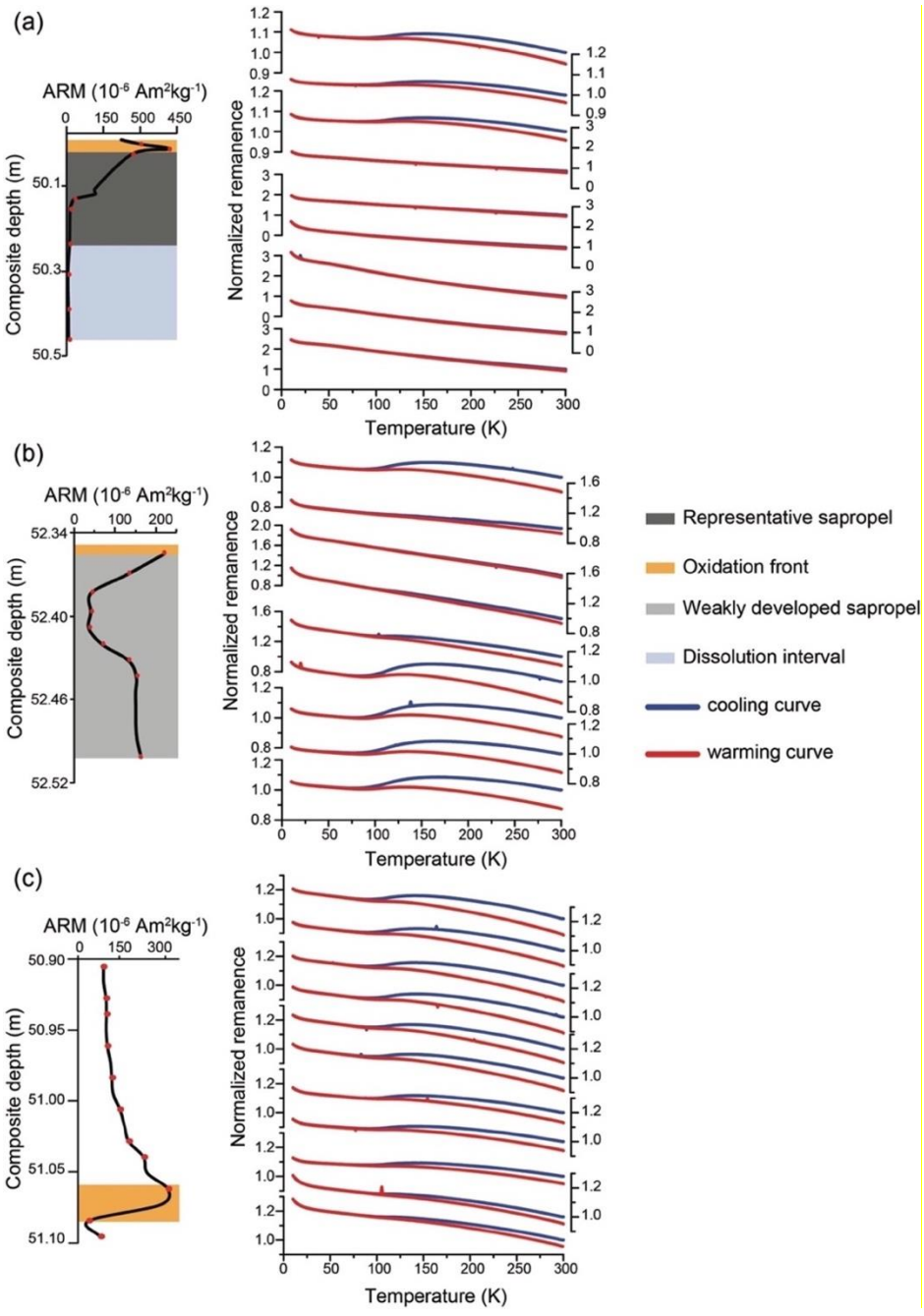

290 **Fig. 6** LTC of RTSIRM for samples (red circles in ARM profiles) selected from (a) a
291 representative sapropel (left), and their corresponding LTC curves (right); (b) as in (a) for a
292 weakly developed sapropel, and (c) as in (a) for marls. Dark gray, light gray, orange, and blue
293 shadings correspond to the representative sapropel, weakly developed sapropel, oxidation
294 front, and dissolution intervals, respectively.
295

296 **6.2.2 Low-temperature cycling of RTSIRM**

297 LTC results for a RTSIRM for the three studied intervals are shown in Fig. 6. Two
298 distinctive LTC-RTSIRM patterns are observed in the representative sapropel (Fig. 6a), with
299 samples from the representative sapropel and dissolution interval having different LTC
300 behavior to the oxidation front (Fig. 6a). In the oxidation front, the remanence increases with
301 cooling before decreasing to a local minimum (typically around 42 K), with a further slight
302 increase at the lowest temperatures. The warming curves are similar to the cooling curves
303 with <5% remanence loss between cooling and warming. Humped curves were observed by
304 Özdemir & Dunlop (2010) for partially oxidized synthetic magnetite. The highest
305 temperature of the hump varies between ~150 and 200 K for both warming and cooling
306 curves (Fig. 6a). Samples from the sapropel and dissolution interval have almost reversible
307 LTC curves, which increase (decrease) during cooling (warming) (Fig. 6a). As reported by
308 Özdemir & Dunlop (2010), such cooling and warming curves are indicative of the occurrence
309 of SSD maghemite. In the lower part of the weakly developed sapropel, LTC-RTSIRM
310 curves are humped. This feature is absent from curves in the upper portion of the weakly
311 developed sapropel (Fig. 6b). Samples from normal marly sediments that were deposited
312 under oxic conditions have different LTC-RTSIRM behavior to the representative sapropel
313 and weakly developed sapropel (Fig. 6c). The hump-shaped feature is present in cooling
314 curves but is absent from warming curves. The Verwey transition is not evident in warming

curves for the marls, which is probably due to maghemitization.

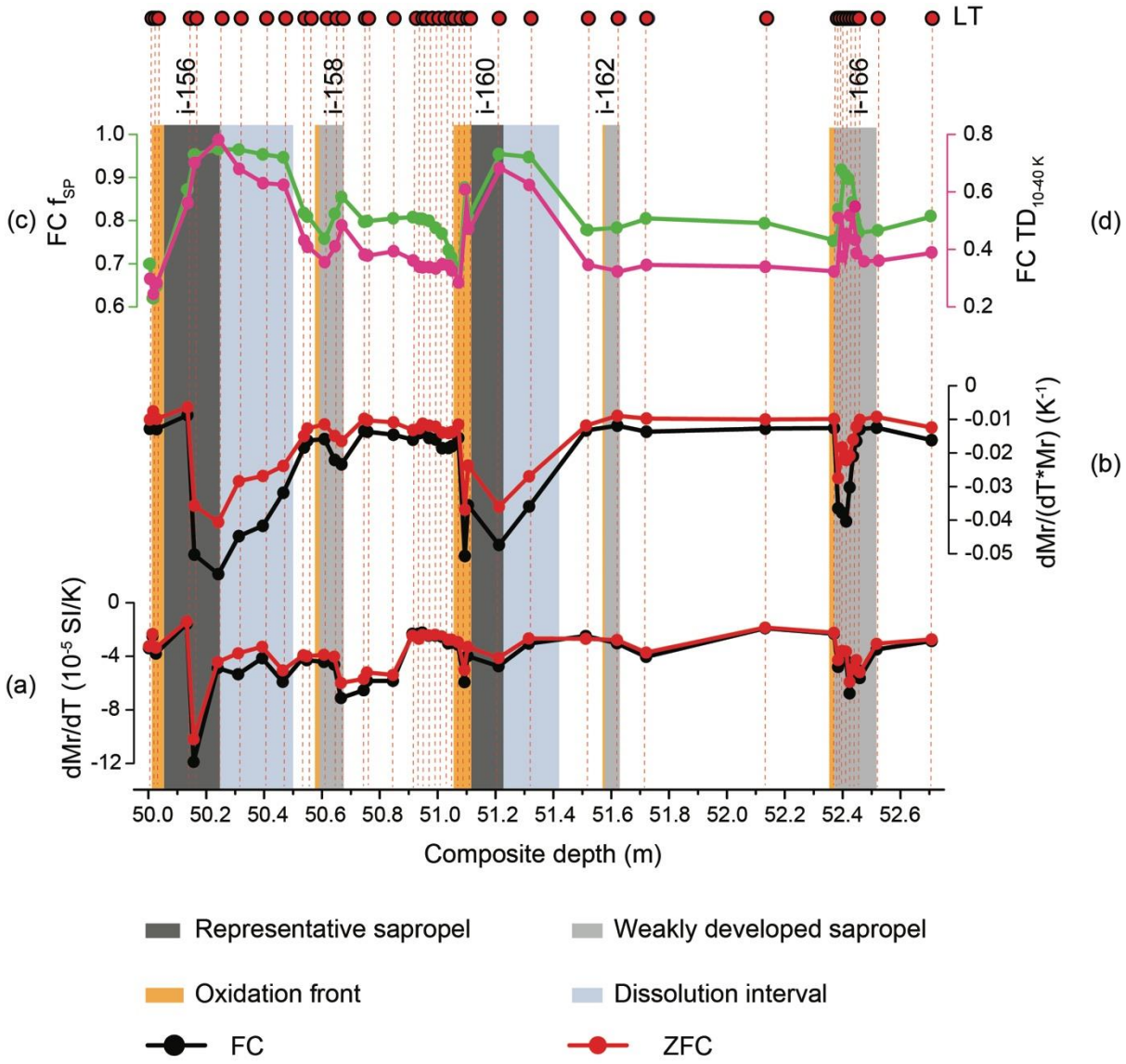

Fig. 7 Quantification of SP particle contents from LT magnetic measurements. (a) Estimation of SP contents from unblocking of ZFC and FC curves, as indicated from dM_r/dT data, which correspond to the absolute initial slope of warming curves; (b) ZFC and FC $(dM_r/dT)/M_r$ data, which correspond to the relative initial slope of warming curves, and (c, d) f_{SP} and $TD_{10\text{-}40K}$ from FC curves, which reflect the importance of SP grains. Dark gray, light gray, orange, and light blue shadings indicate representative sapropels, weakly developed sapropels, oxidation fronts, and dissolution intervals, respectively.

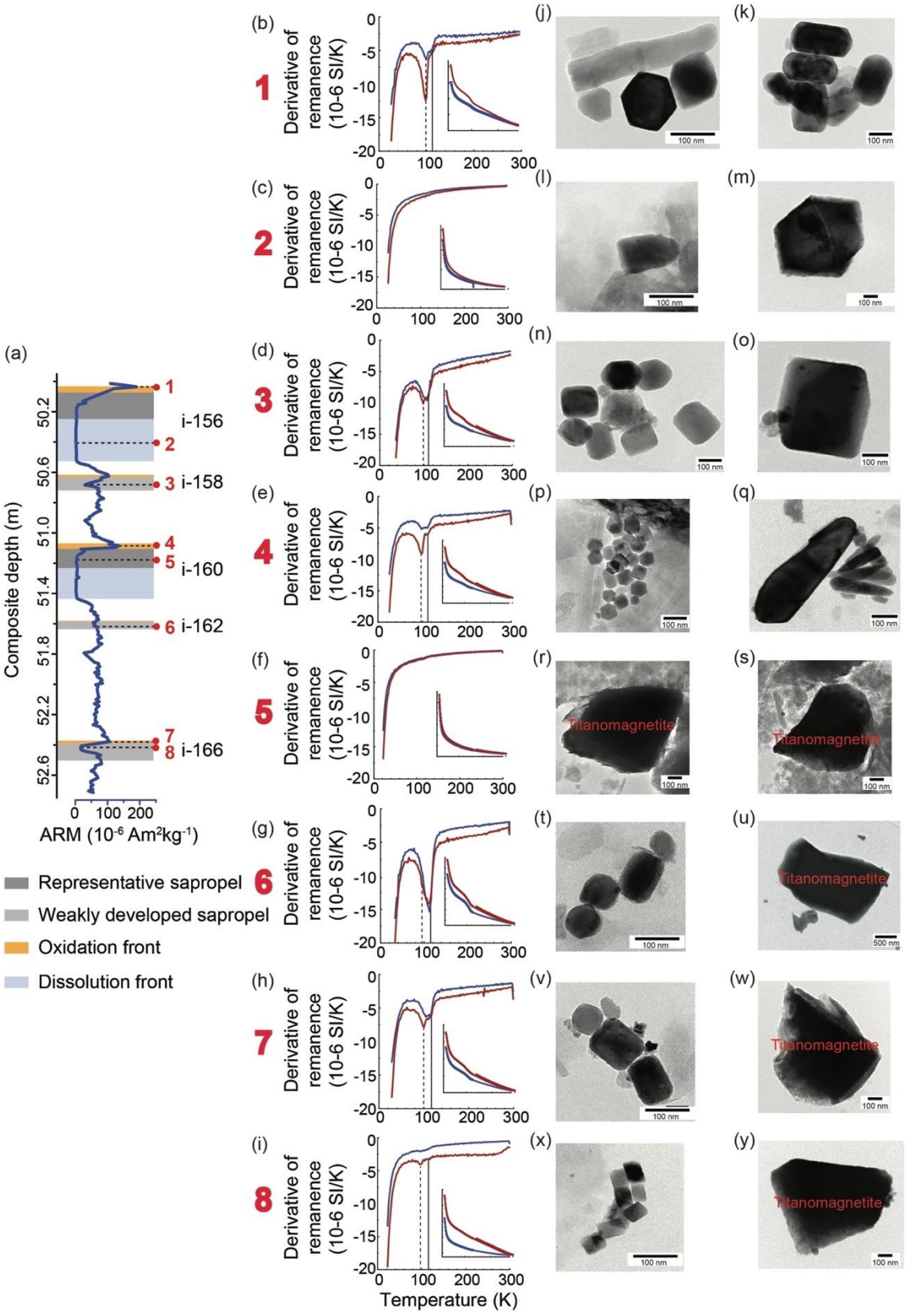

Fig. 8 LT magnetic measurements for eight representative samples and associated TEM images. (a) ARM profile with the eight selected sample positions indicated. (b-i) LT

magnetization curves (inset) and their derivatives (ZFC curves (pink) and FC curves (red)). Distinctive double T_v peaks at ~95 and ~110 K are indicated by vertical dashed and solid lines, respectively. (j-y) TEM images for the representative samples, including (j, k) Sample 1: magnetite magnetofossils from the oxidation front above representative sapropel i-156; (l, m) Sample 2: magnetite magnetofossils and detrital titanomagnetite from the (middle) dissolution zone for representative sapropel i-156; (n, o) Sample 3: magnetite magnetofossils and detrital titanomagnetite from the middle of weakly developed sapropel i-158; (p, q) Sample 4: abundant magnetite magnetofossils from the oxidation front at the top of representative sapropel i-160; (r, s) Sample 5: detrital titanomagnetite from the middle of representative sapropel i-160; (t, u) Sample 6: magnetite magnetofossils and titanomagnetite from the middle of weakly developed sapropel i-162; (v, w) Sample 7: abundant magnetite magnetofossils and detrital titanomagnetite from the oxidation front of weakly developed sapropel i-166; and (x, y) Sample 8: abundant magnetite magnetofossils and detrital titanomagnetite from the middle of weakly developed sapropel i-166. Modified and expanded with additional data from Qian et al. (2020).

7. Discussion

7.1 SP particles

LT measurements are particularly useful for detecting SP particle contents (e.g., Chang et al., 2013; Dearing et al., 1997; Passier & Dekkers, 2002; Roberts, 1995; Smirnov & Tarduno, 2001). The initial slopes of ZFC and FC warming curves are mainly affected by ultrafine grained mineral phases, which unblock at low temperatures between ~10 and 40 K (Banerjee et al., 1993; Özdemir et al, 1993). This SP fraction may come from partial surface oxidation of fine magnetite particles after sapropel formation (Özdemir & Dunlop, 2010).

Thus, $TD_{10\text{-}40K}$, which is equal to $[M_{rs}^{10K} - M_{rs}^{40K}]/M_{rs}^{10K}$ from FC curves, is used to represent the SP content. Moreover, as indicated by the remanence loss between low and room temperature in samples that lack a Verwey transition, the SP fraction (f_{SP}) can be estimated by the relationship (cf. Dunlop, 1973; Roberts, 1995):

$$f_{SP} = \frac{M_{rs}\,(10\,K) - M_{rs}\,(300\,K)}{M_{rs}\,(10\,K)}, \quad (1)$$

where warming occurs in zero field. As discussed in Section 3.1, these estimates may be influenced by paramagnetic magnetizations produced by residual fields in the MPMS superconducting magnet. Such spurious paramagnetic contributions are likely to be stronger in samples with low ferrimagnetic mineral concentrations. This caveat must be considered, although $TD_{10\text{-}40K}$ and f_{SP} are expected here to be mainly indicative of SP content.

Our LT curves have strong remanence losses, which we interpret to be indicative of SP unblocking in ZFC and FC curves below 40 K (Fig. 5). The parameter dM_r/dT provides a measure of the initial slope of ZFC and FC curves. It has relatively low values in dissolution intervals and, thus, does not have a strong expression compared to other SP proxies that focus on relative SP contributions (Fig. 7). To overcome this issue, we normalized the initial slope by M_r to give $(dM_r/dT)/M_r$. Based on steep initial gradients of ZFC and FC curves and the highest values of f_{SP} and $TD_{10\text{-}40\ K}$ results, the SP particle content is higher at the base of representative sapropels and in the middle of weakly developed sapropels compared to other parts of the studied interval (Fig. 7). Although grain size decreases (e.g., ARM/SIRM) within strong dissolution intervals indicate removal of fine-grained material, SP particles do not influence such remanence-based ratios. Previous studies have suggested that SP behavior in diagenetically reduced sediments can have several origins: small immature magnetosomal magnetite crystals, fractions of ultrafine detrital oxidized/unoxidized magnetite, and dissolved ultrafine magnetic particles (Smirnov & Tarduno, 2000; Tarduno, 1995). SP grains may occur as a product of the breakdown of larger SD or vortex state particles in magnetic

mineral reduction zones and may also be precipitated by dissimilatory iron-bearing bacteria (e.g., Moskowitz et al., 1993). Magnetosomal greigite has distinctive magnetic properties (e.g., Reinholdsson et al., 2013) that have so far only been documented in sapropels with extremely high organic carbon levels (Roberts et al., 1999; Type 1 according to Larrasoaña et al. (2003b)), so the presence of fine biogenic greigite is unlikely. High SP contents in the dissolution interval could be due to inorganic SP greigite growth as has been observed widely elsewhere (e.g., Rowan et al., 2009; Roberts et al., 2018). In contrast, the steep initial ZFC and FC slopes in oxidation fronts are likely to have been caused by precipitation of fine-grained iron oxides in the SP state. Despite uncertainty concerning the origin of these hyperfine SP particles, LT measurements enable identification of their presence and can be used to investigate processes responsible for their presence.

7.2. Magnetofossils

Magnetotactic bacteria (MTB) produce highly crystalline SD magnetite within their cells. These particles typically consist of linear chains of SD magnetite, although other structures also occur (Li et al., 2020b, 2020c). After death, the magnetic remains of MTB (referred to as magnetofossils) can contribute to the natural remanent magnetization of sediments (Heslop et al., 2013; Kopp & Kirschvink, 2008; Moisescu et al., 2014; Moskowitz et al., 1993; Roberts et al., 2012). Furthermore, given the link between MTB and specific habitat conditions, magnetofossils can potentially record environmental variability (Chang et al., 2018; Heslop et al., 2014; Hesse, 1994; Li et al., 2013a; Yamazaki, 2008; Yamazaki & Ikehara, 2012).

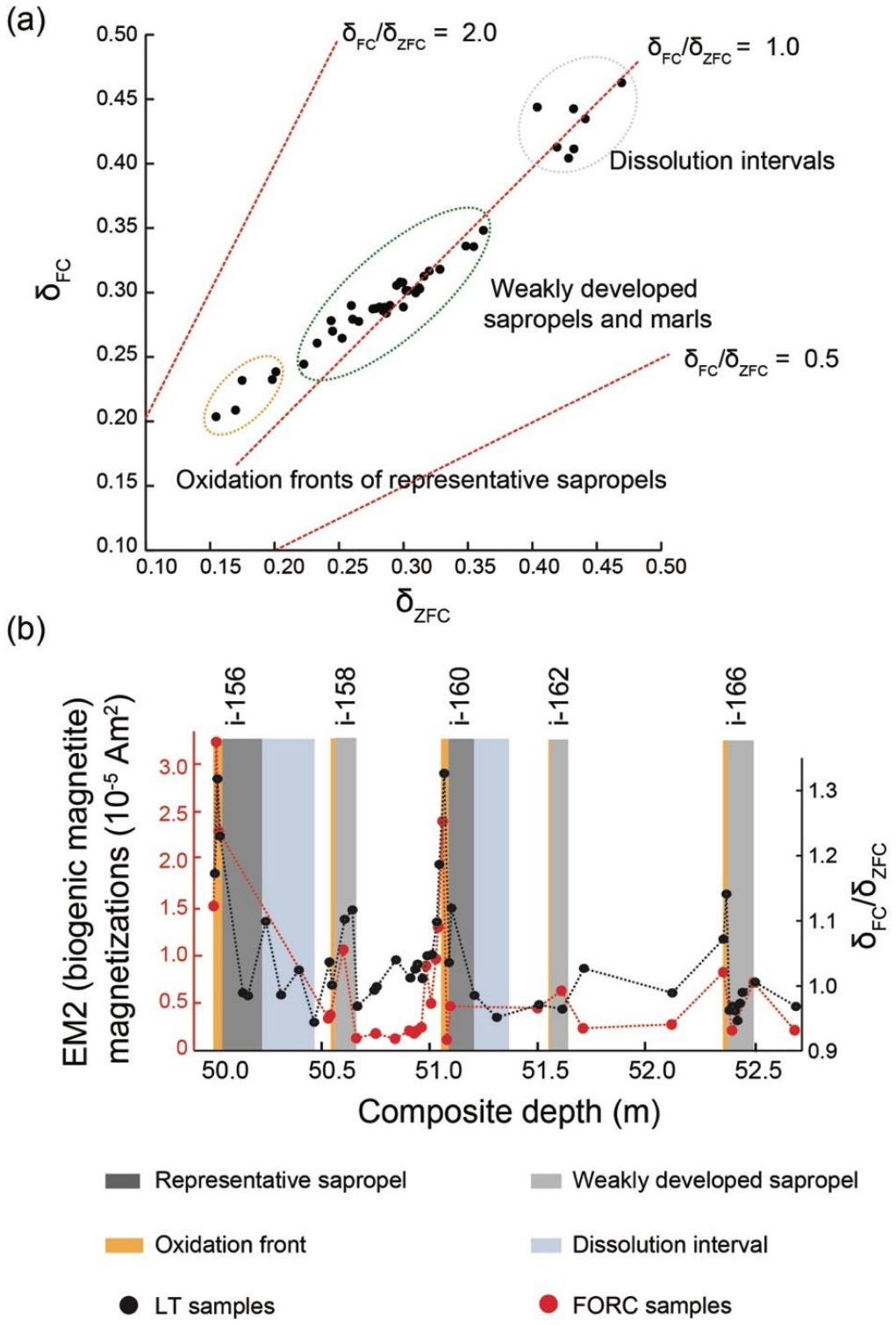

Fig. 9 Moskowitz test results: (a) δ_{FC} versus δ_{ZFC} for all measured samples, and (b) EM2 abundance from the FORC-PCA analysis of Qian et al. (2020), which corresponds to the magnetization due to biogenic magnetite, compared to δ_{FC}/δ_{ZFC} values. Dark gray, light gray,

403 orange, and light blue shadings indicate representative sapropels, weakly developed
404 sapropels, oxidation fronts, and dissolution intervals, respectively.
405
406 LT measurements, particularly FC and ZFC curves, have been used extensively to
407 detect magnetofossils in sediments. The δ_{FC}/δ_{ZFC} parameter has been proposed to detect
408 magnetofossils (Moskowitz et al., 1993), where δ is the remanence lost during warming
409 across the Verwey transition ($\delta = (M_r^{80K} - M_r^{150K})/M_r^{80K}$). When $\delta_{FC}/\delta_{ZFC} > 2$, magnetosome
410 chains may be intact and unoxidized. When δ_{FC}/δ_{ZFC} ~1, magnetosome chains may be
411 disrupted, maghemitized, or occur as part of a mixed magnetic mineral assemblage
412 (Moskowitz et al., 1993). Based on systematic studies of diverse modern MTB and various
413 spatial arrangements of magnetosomal magnetic particles, δ_{ZFC} versus δ_{FC}/δ_{ZFC} (i.e., a so-
414 called δ-plot) has been proposed for identifying unoxidized magnetofossils based on the
415 distribution of magnetosome chains (Li et al., 2012, 2013b, 2020b). From LT analysis of
416 sapropel S1, Passier & Dekkers (2002) interpreted magnetofossils to occur predominantly in
417 oxidized intervals above sapropels.
418 Our LT results indicate that magnetite magnetofossils occur in the studied interval.
419 Double T_v features are present in samples from oxidation fronts, weakly developed sapropels,
420 and marls, but are not found in sediments from strong dissolution intervals. This suggests that
421 magnetofossils exist widely in the studied sediments (Chang et al., 2016), with the exception
422 of zones that have experienced strong magnetite dissolution. TEM images support this
423 hypothesis (Figs. 8j, k, n, p, q, t, v, x, and S2). The lower T_v for biogenic magnetite has been
424 proposed to be an intrinsic property of biogenic magnetite (Pan et al., 2005). Thus,
425 identification of a ~95 K T_v in FC curves appears to be a powerful indicator of the presence
426 of magnetofossils. Moreover, FC remanence loss is more pronounced at ~95 K (biogenic

magnetite) compared to that at ~110 K (inorganic magnetite). The suppressed magnitude of the Verwey transition in inorganic magnetite may be due to Ti substitution in titanomagnetite.

Differences in shape and crystalline anisotropy cause different remanence losses at T_v for biogenic and inorganic magnetite (Moskowitz et al., 1993). The δ parameter quantifies remanence loss during warming through T_v. Although δ_{FC}/δ_{ZFC} does not vary significantly in the studied sediments, the data can be separated into three groups based on sediment type (Fig. 9a). This indicates that biogenic and inorganic magnetite proportions vary between the sediment types. Qian et al. (2020) used FORC-principal component analysis (FORC-PCA) to identify and quantify detrital (EM1) and biogenic (EM2) magnetite in the studied interval. They found that biogenic magnetite is present widely throughout the studied interval and has markedly enhanced concentrations at oxidation fronts, while detrital magnetite dominates the sediment magnetization elsewhere (Qian et al., 2020). Similar stratigraphic variations between EM2 in the FORC-PCA analysis of Qian et al. (2020) and δ_{FC}/δ_{ZFC} indicate that oxidation fronts are dominated by magnetofossils, while weakly developed sapropels and intercalated marls contain mixtures of magnetofossils and inorganic magnetite (Fig. 9b). This interpretation is confirmed by widespread double T_v features in samples selected from weakly developed sapropels and intercalated marls (Chang et al., 2016). δ_{FC}/δ_{ZFC} values for our samples are relatively low (<1.4), which may be due to surface oxidation of magnetofossils or disrupted chains (Chang et al., 2013; Housen & Moskowitz, 2006; Li et al., 2010; Moskowitz et al., 1993; Passier & Dekkers, 2002; Roberts et al., 2012; Smirnov & Tarduno, 2000; Weiss et al., 2004).

7.3. Maghemitization

Although the Verwey transition is not observed in representative sapropels and dissolution intervals, TEM observations demonstrate that magnetofossils and titanomagnetite particles are present (Fig. 9l, m, r, and s). This lack of a T_v signal could be caused either by

partial magnetite oxidation or Ti substitution, which both suppress the Verwey transition, or by a low magnetofossil concentration due to dilution by organic matter or reductive dissolution. Partial magnetite oxidation (maghemitization) is common in marine sediments (Henshaw & Merrill, 1980; Karlin, 1990; Roberts, 2015; Smirnov & Tarduno, 2002; Torii 1997; Vali & Kirschvink, 1989; Yamazaki & Solheid, 2011) and can occur both at the water-sediment interface as a result of diffusion of molecular oxygen into particle surfaces and deeper in the suboxic zone of sediments as a result of bacterially mediated processes that include nitrate reduction (Kïg et al., 1997; Smirnov & Tarduno, 2000; Torii, 1997). Magnetite oxidation can affect low-temperature magnetic properties significantly, including the Verwey transition magnitude, which compromises its detectability (Özdemir et al., 1993). Thus, maghemitization is an important process to consider in environmental magnetic reconstructions.

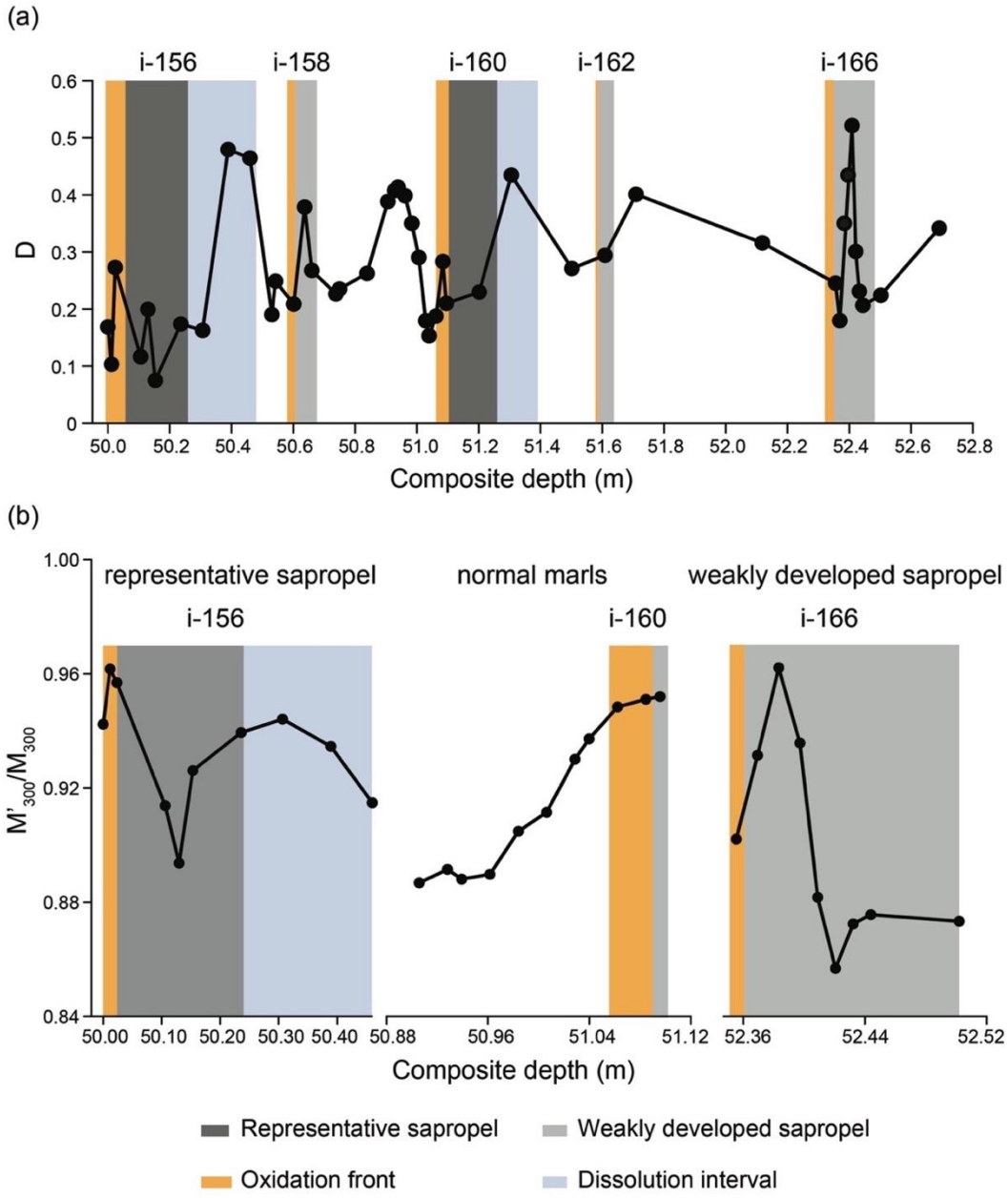

464

465 **Fig. 10** (a) D parameter and (b) M'_{300}/M_{300} as a function of depth in the studied intervals.
466 These parameters indicate the relative importance of maghemitization (partial surface
467 oxidation of magnetite). Dark gray, light gray, orange, and light blue shadings indicate
468 representative sapropels, weakly developed sapropels, oxidation fronts, and dissolution
469 intervals, respectively.

470

471 A distinctive feature of partially oxidized magnetite is the reversible hump in LTC-
472 RTSIRM cooling and warming curves (Chang et al., 2013; Özdemir & Dunlop, 2010).

During cooling, remanence increases between 300 and ~150 K and then decreases dramatically as T_v is approached. During warming, the curves are reversible. When they approach T_v, there is a modest remanence recovery above T_v, and a compensating loss as 300 K is approached. Humped curves are common in the studied sediments, except for the lower part of representative sapropels, underlying magnetite dissolution intervals, and the upper zone of weakly developed sapropels. Within the strong dissolution zones, no T_v is observed in LTC-RTSIRM and ZFC/FC SIRM curves, which suggests the absence of stoichiometric magnetite, and the lack of humped LT-SIRM curves indicates a lack of maghemitization. However, TEM observations (Qian et al. 2020) provide clear evidence that magnetite is still present in these zones, albeit in low concentrations (Fig. 8l and m). Thus, the absence of a detectable Verwey transition is likely indicative of a low magnetite concentration. The room temperature memory ratio, M'_{300}/M_{300}, where M_{300} is the initial M_r at 300 K, and M'_{300} is the terminal M_r value after LT cycling, is an important indicator of partially oxidized magnetite. M'_{300}/M_{300} increases with oxidation degree (Muxworthy et al., 2003; Özdemir & Dunlop, 2010). The memory ratio suggests that oxidized magnetite has minimum abundances in strong dissolution intervals, and maximum abundances in oxidation fronts of representative sapropels (Fig. 10b). For magnetite dissolution intervals, relatively higher M'_{300}/M_{300} values are observed in the lower parts (Fig. 10b), where magnetic mineral abundances are low and iron oxide dissolution is not expected to have been as extensive as in more strongly sulfidized intervals within and immediately below the representative sapropels. This suggests that a fraction of maghemitized magnetite remains in the less extensively sulfidized lower magnetite dissolution interval.

Magnetic memory increases with decreasing grain size in submicron and larger stoichiometric magnetite (Dunlop & Argyle, 1991; Halgedahl & Jarrard, 1995; Hartstra, 1982; Heider et al., 1992; Hodych, 1991; Muxworthy et al., 2003; Özdemir et al., 1993). Finer

498 particles are expected to be affected most by maghemitization because oxidation starts from
499 the surface and proceeds inward, which produces an oxidized shell and a mostly unoxidized
500 core. Fine-grained biogenic magnetite is enriched in oxidation fronts, especially in
501 representative sapropels (Qian et al., 2020), which supports this interpretation. Thus, high
502 M'_{300}/M_{300} values in oxidation fronts of representative sapropels suggest that magnetofossil
503 surfaces in these zones have been maghemitized extensively.

504 Room temperature memory is an indicator of oxidation degree. However, due to
505 lattice mismatch at the maghemite-magnetite interface, the internal stress between the outer
506 maghemite shell and magnetite core could affect remanence recovery when cycling through
507 T_v (Özdemir & Dunlop, 2010), leading to lower M'_{300}/M_{300} values. To avoid the influence of
508 the Verwey transition, Passier & Dekkers (2002) introduced a parameter,
509 $D = \frac{M_{rs\,FC}^{150-300K} - M_{rs\,ZFC}^{150-300K}}{M_{rs\,FC}^{300K}}$, which quantifies the relative difference between the high
510 temperature regions (150-300 K) of FC and ZFC warming curves. Across this high-
511 temperature interval, ZFC and FC curves for unoxidized biogenic magnetite should coincide
512 approximately. Therefore, differences between ZFC and FC curves in this high-temperature
513 interval may be caused by oxidation of detrital magnetite (Passier & Dekkers, 2002; Smirnov
514 & Tarduno, 2000). Low *D* values are observed in the representative sapropels and in the
515 upper to middle dissolution intervals (Fig. 10a), which indicates a low degree of magnetite
516 oxidation. This is consistent with the expectation that maghemitized shells in partially
517 oxidized magnetite dissolve before the magnetite core of such composite core-shell particles
518 (Torii, 1997; Yamazaki & Solheid, 2011).
519

8. Conclusions

Low-temperature magnetic analysis of sediments can provide valuable insights into processes of importance in environmental magnetism. Our results indicate that superparamagnetic particle contents are elevated in the lower part of representative sapropels and in the middle of weakly developed sapropels. Double T_v features in ZFC and FC warming curves suggest that magnetite magnetofossils and detrital magnetite occur widely in the studied sediments except within representative sapropels and their underlying dissolution intervals. In addition, we demonstrate that maghemitization is a common phenomenon in the studied oxic sediment intervals, which suggests that magnetite magnetofossils have experienced surficial maghemitization. The sensitivity of LT magnetic analyses to important environmental processes suggests that they deserve to be used more extensively in environmental magnetism for detecting magnetofossils, SP particles, and maghemitization on magnetite particle surfaces.

Acknowledgements

This work was supported financially by the Australian Research Council (grants DP160100805 and DP200100765) and the National Natural Science Foundation of China (grants 41920104009 and 41890843). Yao Qian is supported by the China Scholarship Council for her PhD study at ANU. We thank Mrs. Lixin Gu and Tang Xu for helping with TEM measurements. Data can be found in the RMAG portal (rock magic database) of the Magnetics Information Consortium via the link http://earthref.org/MAGIC/.

References

Amies, J. D., Rohling, E. J., Grant, K. M., Rodríguez-Sanz, L., & Marino, G. (2019). Quantification of African monsoon runoff during last interglacial sapropel S5. *Paleoceanography and Paleoclimatology*, *34*(8), 1487-1516. https://doi.org/10.1029/2019PA003652

Banerjee, S. K., Hunt, C. P., & Liu, X. M. (1993). Separation of local signals from the regional paleomonsoon record of the Chinese Loess Plateau: A rock-magnetic approach. *Geophysical Research Letters*, *20*(9), 843-846. https://doi.org/10.1029/93GL00908

Besnus, M. J., & Meyer, A. J. (1964). Nouvelles données expérimentales sur le magnétisme de la pyrrhotine naturelle. *Proceedings of the International Conference on Magnetism, Nottingham*, pp. 507-511.

Bloemendal, J., King, J. W., Hall, F. R., & Doh, S. J. (1992). Rock magnetism of Late Neogene and Pleistocene deep-sea sediments: Relationship to sediment source, diagenetic processes, and sediment lithology. *Journal of Geophysical Research: Solid Earth*, *97*(B4), 4361-4375. https://doi.org/10.1029/91jb03068

Castradori, D. (1993). Calcareous nannofossils and the origin of eastern Mediterranean sapropels. *Paleoceanography*, *8*(4), 459-471. https://doi.org/10.1029/93PA00756

Chang, L., Harrison, R. J., Zeng, F., Berndt, T. A., Roberts, A. P., Heslop, D., & Zhao, X. (2018). Coupled microbial bloom and oxygenation decline recorded by magnetofossils during the Palaeocene-Eocene Thermal Maximum. *Nature Communications*, *9*(1), 1-9. https://doi.org/10.1038/s41467-018-06472-y

Chang, L., Heslop, D., Roberts, A. P., Rey, D., & Mohamed, K. J. (2016). Discrimination of biogenic and detrital magnetite through a double Verwey transition temperature. *Journal of Geophysical Research: Solid Earth*, *121*(1), 3-14. https://doi.org/10.1002/2015jb012485

Chang, L., Winklhofer, M., Roberts, A. P., Heslop, D., Florindo, F., Dekkers, M. J., et al. (2013). Low-temperature magnetic properties of pelagic carbonates: Oxidation of biogenic magnetite and identification of magnetosome chains. *Journal of Geophysical Research: Solid Earth*, *118*(12), 6049-6065. https://doi.org/10.1002/2013JB010381

Coulthard, T. J., Ramirez, J. A., Barton, N., Rogerson, M., & Brücher, T. (2013). Were rivers flowing across the Sahara during the last interglacial? Implications for human

migration through Africa. *PloS one*, *8*(9), e74834. https://doi.org/10.1371/annotation/0a0303fa-ae35-4100-9f8d-c9ad65d49897

Dearing, J. A., Bird, P. M., Dann, R. J. L., & Benjamin, S. F. (1997). Secondary ferrimagnetic minerals in Welsh soils: A comparison of mineral magnetic detection methods and implications for mineral formation. *Geophysical Journal International*, *130*(3), 727-736. https://doi.org/10.1111/j.1365-246X.1997.tb01867.x

Dekkers, M. J., Langereis, C. G., Vriend, S. P., van Santvoort, P. J. M., & de Lange, G. J. (1994). Fuzzy *c*-means cluster analysis of early diagenetic effects on natural remanent magnetisation acquisition in a 1.1 Myr piston core from the Central Mediterranean. *Physics of the Earth and Planetary Interiors*, *85*(1-2), 155-171. https://doi.org/10.1016/0031-9201(94)90014-0

Dekkers, M. J., Mattéi, J. L., Fillion, G., & Rochette, P. (1989). Grain-size dependence of the magnetic behavior of pyrrhotite during its low-temperature transition at 34 K. *Geophysical Research Letters*, *16*(8), 855-858. https://doi.org/10.1029/GL016i008p00855

Drake, N. A., Breeze, P., & Parker, A. (2013). Palaeoclimate in the Saharan and Arabian Deserts during the Middle Palaeolithic and the potential for hominin dispersals. *Quaternary International*, *300*, 48-61. https://doi.org/10.1016/j.quaint.2012.12.018

Dunlop, D. J. (1973). Superparamagnetic and single-domain threshold sizes in magnetite. *Journal of Geophysical Research*, *78*(11), 1780-1793. https://doi.org/10.1029/JB078i011p01780

Dunlop, D. J., & Argyle, K. S. (1991). Separating multidomain and single-domain-like remanences in pseudo-single-domain magnetites (215-540 nm) by low-temperature demagnetization. *Journal of Geophysical Research: Solid Earth*, *96*(B2), 2007-2017. https://doi.org/10.1029/90JB02338

Emeis, K. C., Sakamoto, T., Wehausen, R., & Brumsack, H. J. (2000a). The sapropel record of the eastern Mediterranean Sea - results of Ocean Drilling Program Leg 160. *Palaeogeography, Palaeoclimatology, Palaeoecology*, *158*(3-4), 371-395. https://doi.org/10.1016/S0031-0182(00)00059-6

Emeis, K. C., Struck, U., Schulz, H. M., Rosenberg, R., Bernasconi, S., Erlenkeuser, H., et al. (2000b). Temperature and salinity variations of Mediterranean Sea surface waters over the last 16,000 years from records of planktonic stable oxygen isotopes and

alkenone unsaturation ratios. *Palaeogeography, Palaeoclimatology, Palaeoecology*, *158*(3-4), 259-280. https://doi.org/10.1016/S0031-0182(00)00053-5

Emeis, K. C., Schulz, H., Struck, U., Rossignol-Strick, M., Erlenkeuser, H., Howell, M. W., et al. (2003). Eastern Mediterranean surface water temperatures and $\delta^{18}O$ composition during deposition of sapropels in the late Quaternary. *Paleoceanography*, *18*(1). https://doi.org/10.1029/2000PA000617

Garming, J. F. L., de Lange, G. J., Dekkers, M. J., & Passier, H. F. (2004). Changes in magnetic parameters after sequential iron phase extraction of eastern Mediterranean sapropel S1 sediments. *Studia Geophysica et Geodaetica*, *48*(2), 345-362. https://doi.org/10.1023/b:sgeg.0000020837.18450.76

Grant, K. M., Grimm, R., Mikolajewicz, U., Marino, G., Ziegler, M., & Rohling, E. J. (2016). The timing of Mediterranean sapropel deposition relative to insolation, sea-level and African monsoon changes. *Quaternary Science Reviews*, *140*, 125-141. https://doi.org/10.1016/j.quascirev.2016.03.026

Grant, K. M., Rohling, E. J., Westerhold, T., Zabel, M., Heslop, D., Konijnendijk, T., & Lourens, L. (2017). A 3 million year index for North African humidity/aridity and the implication of potential pan-African Humid periods. *Quaternary Science Reviews*, *171*, 100-118. https://doi.org/10.1016/j.quascirev.2017.07.005

Halgedahl, S. L., & Jarrard, R. D. (1995). Low-temperature behavior of single-domain through multidomain magnetite. *Earth and Planetary Science Letters*, *130*(1-4), 127-139. https://doi.org/10.1016/0012-821X(94)00260-6

Hartstra, R. L. (1982). Grain-size dependence of initial susceptibility and saturation magnetization-related parameters of four natural magnetites in the PSD-MD range. *Geophysical Journal International*, *71*(2), 477-495. https://doi.org/10.1111/j.1365-246X.1982.tb05998.x

Heider, F., Dunlop, D. J., & Soffel, H. C. (1992). Low-temperature and alternating field demagnetization of saturation remanence and thermoremanence in magnetite grains (0.037 μm to 5 mm). *Journal of Geophysical Research: Solid Earth*, *97*(B6), 9371-9381. https://doi.org/10.1029/91JB03097

Henshaw Jr, P. C., & Merrill, R. T. (1980). Magnetic and chemical changes in marine sediments. *Reviews of Geophysics*, *18*(2), 483-504. https://doi.org/10.1029/RG018i002p00483

Heslop, D., Roberts, A. P., & Chang, L. (2014). Characterizing magnetofossils from first-order reversal curve (FORC) central ridge signatures. *Geochemistry, Geophysics, Geosystems*, *15*(6), 2170-2179. https://doi.org/10.1002/2014GC005291

Heslop, D., Roberts, A. P., Chang, L., Davies, M., Abrajevitch, A., & De Deckker, P. (2013). Quantifying magnetite magnetofossil contributions to sedimentary magnetizations. *Earth and Planetary Science Letters*, *382*, 58-65. https://doi.org/10.1016/j.epsl.2013.09.011

Hesse, P. P. (1994). Evidence for bacterial palaeoecological origin of mineral magnetic cycles in oxic and sub-oxic Tasman Sea sediments. *Marine Geology*, *117*(1-4), 1-17. https://doi.org/10.1016/0025-3227(94)90003-5

Hodych, J. P. (1991). Low-temperature demagnetization of saturation remanence in rocks bearing multidomain magnetite. *Physics of the Earth and Planetary Interiors*, *66*(3-4), 144-152. https://doi.org/10.1016/0031-9201(91)90073-Q

Housen, B. A., & Moskowitz, B. M. (2006). Depth distribution of magnetofossils in near-surface sediments from the Blake/Bahama Outer Ridge, western North Atlantic Ocean, determined by low-temperature magnetism. *Journal of Geophysical Research: Biogeosciences*, *111*(G1). https://doi.org/10.1029/2005jg000068

Housen, B. A., Banerjee, S. K., & Moskowitz, B. M. (1996). Low-temperature magnetic properties of siderite and magnetite in marine sediments. *Geophysical Research Letters*, *23*(20), 2843-2846. https://doi.org/10.1029/96GL01197

Karlin, R. (1990). Magnetite diagenesis in marine sediments from the Oregon continental margin. *Journal of Geophysical Research: Solid Earth*, *95*(B4), 4405-4419. https://doi.org/10.1029/JB095iB04p04405

Kïg, I., Drodt, M., Suess, E., & Trautwein, A. X. (1997). Iron reduction through the tan-green color transition in deep-sea sediments. *Geochimica et Cosmochimica Acta*, *61*(8), 1679-1683. https://doi.org/10.1016/S0016-7037(97)00007-0

King, J. W., & Channell, J. E. T. (1991). Sedimentary magnetism, environmental magnetism, and magnetostratigraphy. *Reviews of Geophysics*, *29*, 358-370. https://doi.org/10.1002/rog.1991.29.s1.358

King, J., Banerjee, S. K., Marvin, J., & Özdemir, Ö. (1982). A comparison of different magnetic methods for determining the relative grain-size of magnetite in natural materials: Some results from lake-sediments. *Earth and Planetary Science Letters*, *59*(2), 404-419. https://doi.org/10.1016/0012-821x(82)90142-X

671 Kopp, R. E., & Kirschvink, J. L. (2008). The identification and biogeochemical interpretation
672 of fossil magnetotactic bacteria. *Earth-Science Reviews*, *86*(1-4), 42-61.
673 https://doi.org/10.1016/j.earscirev.2007.08.001
674 Kruiver, P. P., & Passier, H. F. (2001). Coercivity analysis of magnetic phases in sapropel S1
675 related to variations in redox conditions, including an investigation of the S ratio.
676 *Geochemistry, Geophysics, Geosystems*, *2*(12). https://doi.org/10.1029/2001gc000181
677 Langereis, C. G., & Dekkers M. J. (1999). Magnetic cyclostratigraphy: High-resolution
678 dating in and beyond the Quaternary and analysis of periodic changes in diagenesis
679 and sedimentary magnetism. *Quaternary Climates, Environments and Magnetism*, pp.
680 352-382, eds Maher, B. A. & Thompson, R., Cambridge University Press.
681 Larrasoaña, J. C., Roberts, A. P., Hayes, A., Wehausen, R., & Rohling, E. J. (2006).
682 Detecting missing beats in the Mediterranean climate rhythm from magnetic
683 identification of oxidized sapropels (Ocean Drilling Program Leg 160). *Physics of the*
684 *Earth and Planetary Interiors*, *156*(3-4), 283-293.
685 https://doi.org/10.1016/j.pepi.2005.04.017
686 Larrasoaña, J. C., Roberts, A. P., Musgrave, R. J., Gràcia, E., Piñero, E., Vega, M., &
687 Martínez-Ruiz, F. (2007). Diagenetic formation of greigite and pyrrhotite in gas
688 hydrate marine sedimentary systems. *Earth and Planetary Science Letters*, *261*(3-4),
689 350-366. https://doi.org/10.1016/j.epsl.2007.06.032
690 Larrasoaña, J. C., Roberts, A. P., Rohling, E. J., Winklhofer, M., & Wehausen, R. (2003a).
691 Three million years of monsoon variability over the northern Sahara. *Climate*
692 *Dynamics*, *21*(7-8), 689-698. https://doi.org/10.1007/s00382-003-0355-z
693 Larrasoaña, J. C., Roberts, A. P., Stoner, J. S., Richter, C., & Wehausen, R. (2003b). A new
694 proxy for bottom-water ventilation in the eastern Mediterranean based on
695 diagenetically controlled magnetic properties of sapropel-bearing sediments.
696 *Palaeogeography, Palaeoclimatology, Palaeoecology*, *190*, 221-242.
697 https://doi.org/10.1016/S0031-0182(02)00607-7
698 Li, J., Benzerara, K., Bernard, S., & Beyssac, O. (2013a). The link between biomineralization
699 and fossilization of bacteria: Insights from field and experimental studies. *Chemical*
700 *Geology*, *359*, 49-69. http://dx.doi.org/10.1016/j.chemgeo.2013.09.013
701 Li, J., Ge, K., Pan, Y., Williams, W., Liu, Q., & Qin, H. (2013b). A strong angular
702 dependence of magnetic properties of magnetosome chains: Implications for rock
703 magnetism and paleomagnetism. *Geochemistry, Geophysics, Geosystems*, *14*(10),
704 3887-3907. https://doi.org/10.1002/Ggge.20228

Li, J., Liu, Y., Liu, S., Roberts, A. P., Pan, H., Xiao, T., et al. (2020a). Classification of a complexly mixed magnetic mineral assemblage in Pacific Ocean surface sediment by electron microscopy and supervised magnetic unmixing. *Frontiers in Earth Science*, *8*, 648. https://doi.org/10.3389/feart.2020.609058

Li, J., Menguy, N., Leroy, E., Roberts, A. P., Liu, P., & Pan, Y. (2020b). Biomineralization and magnetism of uncultured magnetotactic coccus strain THC-1 with non-chained magnetosomal magnetite nanoparticles. *Journal of Geophysical Research: Solid Earth*, e2020JB020853. https://doi.org/10.1029/2020JB020853

Li, J., Menguy, N., Roberts, A. P., Gu, L., Leroy, E., Bourgon, J., et al. (2020c). Bullet-shaped magnetite biomineralization within a magnetotactic deltaproteobacterium: Implications for magnetofossil identification. *Journal of Geophysical Research: Biogeosciences*, *125*(7), e2020JG005680. https://doi.org/10.1029/2020jg005680

Li, J., Pan, Y., Liu, Q., Yu-Zhang, K., Menguy, N., Che, R., et al. (2010). Biomineralization, crystallography and magnetic properties of bullet-shaped magnetite magnetosomes in giant rod magnetotactic bacteria. *Earth and Planetary Science Letters*, *293*(3-4), 368-376. https://doi.org/10.1016/j.epsl.2010.03.007

Li, J., Wu, W., Liu, Q., & Pan, Y. (2012). Magnetic anisotropy, magnetostatic interactions and identification of magnetofossils. *Geochemistry, Geophysics, Geosystems*, *13*(12). https://doi.org/10.1029/2012GC004384

Liu, Q. S., Larrasoaña, J. C., Torrent, J., Roberts, A. P., Rohling, E. J., Liu, Z. F., & Jiang, Z. X. (2012). New constraints on climate forcing and variability in the circum-Mediterranean region from magnetic and geochemical observations of sapropels S1, S5 and S6. *Palaeogeography, Palaeoclimatology, Palaeoecology*, *333*, 1-12. https://doi.org/10.1016/j.palaeo.2012.02.036

Lourens, L. J., Wehausen, R., & Brumsack, H. J. (2001). Geological constraints on tidal dissipation and dynamical ellipticity of the Earth over the past three million years. *Nature*, *409*(6823), 1029-1033. https://doi.org/0.1038/35059062

Moisescu, C., Ardelean, I., & Benning, L. G. (2014). The effect and role of environmental conditions on magnetosome synthesis. *Frontiers in Microbiology*, *5*, 49. https://doi.org/10.3389/fmicb.2014.00049

Morin, F. J. (1950). Magnetic susceptibility of αFe_2O_3 and αFe_2O_3 with added titanium. *Physical Review*, *78*(6), 819. https://doi.org/10.1007/bf00308211

Moskowitz, B. M., Frankel, R. B., & Bazylinski, D. A. (1993). Rock magnetic criteria for the detection of biogenic magnetite. *Earth and Planetary Science Letters*, *120*(3-4), 283-300. https://doi.org/10.1016/0012-821X(93)90245-5

Muxworthy, A., Williams, W., & Virdee, D. (2003). Effect of magnetostatic interactions on the hysteresis parameters of single-domain and pseudo-single-domain grains. *Journal of Geophysical Research: Solid Earth*, *108*(B11). https://doi.org/10.1029/2003JB002588

Myers, P. G., Haines, K., & Rohling, E. J. (1998). Modeling the paleocirculation of the Mediterranean: The Last Glacial Maximum and the Holocene with emphasis on the formation of sapropel S1. *Paleoceanography*, *13*(6), 586-606. https://doi.org/10.1029/98PA02736

Osborne, A. H., Vance, D., Rohling, E. J., Barton, N., Rogerson, M., & Fello, N. (2008). A humid corridor across the Sahara for the migration of early modern humans out of Africa 120,000 years ago. *Proceedings of the National Academy of Sciences USA*, *105*(43), 16444-16447. https://doi.org/10.1073/pnas.0804472105

Özdemir, Ö., & Dunlop, D. J. (2010). Hallmarks of maghemitization in low-temperature remanence cycling of partially oxidized magnetite nanoparticles. *Journal of Geophysical Research: Solid Earth*, *115*(B2). https://doi.org/10.1029/2009JB006756

Özdemir, Ö., Dunlop, D. J., & Moskowitz, B. M. (1993). The effect of oxidation on the Verwey transition in magnetite. *Geophysical Research Letters*, *20*(16), 1671-1674. https://doi.org/10.1029/93GL01483

Pan, Y., Petersen, N., Winklhofer, M., Davila, A. F., Liu, Q., Frederichs, T., et al. (2005). Rock magnetic properties of uncultured magnetotactic bacteria. *Earth and Planetary Science Letters*, *237*(3-4), 311-325. https://doi.org/10.1016/j.epsl.2005.06.029

Passier, H. F., & Dekkers, M. J. (2002). Iron oxide formation in the active oxidation front above sapropel S1 in the eastern Mediterranean Sea as derived from low-temperature magnetism. *Geophysical Journal International*, *150*(1), 230-240. https://doi.org/10.1046/j.1365-246X.2002.01704.x

Passier, H. F., de Lange, G. J., & Dekkers, M. J. (2001). Magnetic properties and geochemistry of the active oxidation front and the youngest sapropel in the eastern Mediterranean Sea. *Geophysical Journal International*, *145*(3), 604-614. https://doi.org/10.1046/j.0956-540x.2001.01394.x

769 Pike, C. R., Roberts, A. P., & Verosub, K. L. (1999). Characterizing interactions in fine
770 magnetic particle systems using first order reversal curves. *Journal of Applied*
771 *Physics*, *85*(9), 6660-6667. https://doi.org/10.1063/1.370176
772 Qian, Y., Roberts, A. P., Liu, Y., Hu, P., Zhao, X., Heslop, D., et al. (2020). Assessment and
773 integration of bulk and component-specific methods for identifying mineral magnetic
774 assemblages in environmental magnetism. *Journal of Geophysical Research: Solid*
775 *Earth*, *125*(8), e2019JB019024. https://doi.org/10.1029/2019JB019024
776 Reinholdsson, M., Snowball, I., Zillén, L., Lenz, C., & Conley, D. J. (2013). Magnetic
777 enhancement of Baltic Sea sapropels by greigite magnetofossils. *Earth and Planetary*
778 *Science Letters*, *366*, 137-150. https://doi.org/10.1016/j.epsl.2013.01.029
779 Roberts, A. P. (1995). Magnetic properties of sedimentary greigite (Fe_3S_4). *Earth and*
780 *Planetary Science Letters*, *134*(3), 227-236. https://doi.org/10.1016/0012-
781 821x(95)00131-u
782 Roberts, A. P. (2015). Magnetic mineral diagenesis. *Earth-Science Reviews*, *151*, 1-47.
783 https://doi.org/10.1016/j.earscirev.2015.09.010
784 Roberts, A. P., Chang, L., Heslop, D., Florindo, F., & Larrasoaña, J. C. (2012). Searching for
785 single domain magnetite in the "pseudo-single-domain" sedimentary haystack:
786 Implications of biogenic magnetite preservation for sediment magnetism and relative
787 paleointensity determinations. *Journal of Geophysical Research: Solid Earth*, *117*,
788 B08104. https://doi.org/Artn B0810410.1029/2012jb009412
789 Roberts, A. P., Stoner, J. S., & Richter, C. (1999). Diagenetic magnetic enhancement of
790 sapropels from the eastern Mediterranean Sea. *Marine Geology*, *153*(1-4), 103-116.
791 https://doi.org/10.1016/S0025-3227(98)00087-5
792 Roberts, A. P., Zhao, X., Harrison, R. J., Heslop, D., Muxworthy, A. R., Rowan, C. J.,
793 Larrasoaña, J.-C., & Florindo, F. (2018). Signatures of reductive magnetic mineral
794 diagenesis from unmixing of first-order reversal curves. *Journal of Geophysical*
795 *Research: Solid Earth*, *121*, 4500-4522.
796 Robinson, S. G., Sahota, J. T., & Oldfield, F. (2000). Early diagenesis in North Atlantic
797 abyssal plain sediments characterized by rock-magnetic and geochemical indices.
798 *Marine Geology*, *163*(1-4), 77-107. https://doi.org/10.1016/S0025-3227(99)00108-5
799 Rochette, P., Fillion, G., & Dekkers, M. J. (2011). Interpretation of low-temperature data part
800 4: the low-temperature magnetic transition of monoclinic pyrrhotite. *The IRM*
801 *Quarterly*, *21*(1), 1-7.

Rochette, P., Fillion, G., Mattéi, J. L., & Dekkers, M. J. (1990). Magnetic transition at 30-34 Kelvin in pyrrhotite: Insight into a widespread occurrence of this mineral in rocks. *Earth and Planetary Science Letters*, *98*(3-4), 319-328. https://doi.org/10.1016/0012-821X(90)90034-U

Rohling, E. J. (1994). Review and new aspects concerning the formation of Eastern Mediterranean sapropels. *Marine Geology*, *122*(1-2), 1-28. https://doi.org/10.1016/0025-3227(94)90202-X

Rohling, E. J. (1999). Environmental control on Mediterranean salinity and $\delta^{18}O$. *Paleoceanography*, *14*(6), 706-715. https://doi.org/10.1029/1999PA900042

Rohling, E. J., & Gieskes, W. W. (1989). Late Quaternary changes in Mediterranean intermediate water density and formation rate. *Paleoceanography*, *4*(5), 531-545. https://doi.org/10.1029/PA004i005p00531

Rohling, E. J., Cane, T. R., Cooke, S., Sprovieri, M., Bouloubassi, I., Emeis, K. C., et al. (2002). African monsoon variability during the previous interglacial maximum. *Earth and Planetary Science Letter*s, *202*(1), 61-75. https://doi.org/10.1016/S0012-821X(02)00775-6

Rohling, E. J., Foster, G. L., Grant, K. M., Marino, G., Roberts, A. P., Tamisiea, M. E., et al. (2014). Sea-level and deep-sea-temperature variability over the past 5.3 million years. *Nature*, *508*(7497), 477-482. https://doi.org/10.1038/nature13230

Rohling, E. J., Sprovieri, M., Cane, T., Casford, J. S., Cooke, S., Bouloubassi, I., et al. (2004). Reconstructing past planktic foraminiferal habitats using stable isotope data: A case history for Mediterranean sapropel S5. *Marine Micropaleontology*, *50*(1-2), 89-123. https://doi.org/10.1016/S0377-8398(03)00068-9

Rossignol-Strick, M. (1983). African monsoons, an immediate climate response to orbital insolation. *Nature*, *304*(5921), 46-49. https://doi.org/10.1038/304046a0

Rossignol-Strick, M. (1985). Mediterranean Quaternary sapropels, an immediate response of the African monsoon to variation of insolation. *Palaeogeography, Palaeoclimatology, Palaeoecology*, *49*(3-4), 237-263. https://doi.org/10.1016/0031-0182(85)90056-2

Rossignol-Strick, M. (1987). Rainy periods and bottom water stagnation initiating brine accumulation and metal concentrations: 1. The late Quaternary. *Paleoceanography*, *2*(3), 333-360. https://doi.org/10.1029/PA002i003p00333

Rossignol-Strick, M., Nesteroff, W., Olive, P., & Vergnaud-Grazzini, C. (1982). After the deluge: Mediterranean stagnation and sapropel formation. *Nature*, *295*(5845), 105-110. https://doi.org/10.1038/295105a0

Rowan, C. J., Roberts, A. P., & Broadbent, T. (2009). Reductive diagenesis, magnetite dissolution, greigite growth and paleomagnetic smoothing in marine sediments: A new view. *Earth and Planetary Science Letters*, *277*(1-2), 223-235. https://doi.org/10.1016/j.epsl.2008.10.016

Scrivner, A. E., Vance, D., & Rohling, E. J. (2004). New neodymium isotope data quantify Nile involvement in Mediterranean anoxic episodes. *Geology*, *32*(7), 565-568. https://doi.org/10.1130/G20419.1

Smirnov, A. V., & Tarduno, J. A. (2000). Low-temperature magnetic properties of pelagic sediments (Ocean Drilling Program Site 805C): Tracers of maghemitization and magnetic mineral reduction. *Journal of Geophysical Research: Solid Earth*, *105*(B7), 16457-16471. https://doi.org/10.1029/2000JB900140

Smirnov, A. V., & Tarduno, J. A. (2001). Estimating superparamagnetism in marine sediments with the time dependency of coercivity of remanence. *Journal of Geophysical Research: Solid Earth*, *106*(B8), 16135-16143. https://doi.org/10.1029/2001JB000152

Smirnov, A. V., & Tarduno, J. A. (2002). Magnetic field control of the low-temperature magnetic properties of stoichiometric and cation-deficient magnetite. *Earth and Planetary Science Letters*, *194*(3-4), 359-368. https://doi.org/10.1016/S0012-821X(01)00575-1

Tarduno, J. A. (1995). Superparamagnetism and reduction diagenesis in pelagic sediments: Enhancement or depletion? *Geophysical Research Letters*, *22*(11), 1337-1340. https://doi.org/10.1029/95GL00888

Tarduno, J. A., & Wilkison, S. L. (1996). Non-steady state magnetic mineral reduction, chemical lock-in, and delayed remanence acquisition in pelagic sediments. *Earth and Planetary Science Letters*, *144*(3-4), 315-326. https://doi.org/10.1016/S0012-821X(96)00174-4

Torii, M. (1997). Low-temperature oxidation and subsequent downcore dissolution of magnetite in deep-sea sediments, ODP Leg 161 (Western Mediterranean). *Journal of Geomagnetism and Geoelectricity*, *49*(10), 1233-1245. https://doi.org/10.5636/jgg.49.1233

Vali, H., & Kirschvink, J. L. (1989). Magnetofossil dissolution in a palaeomagnetically unstable deep-sea sediment. *Nature*, *339*(6221), 203-206. https://doi.org/10.1038/339203a0

van Hoof, A. A. M., Van Os, B. J. H., Rademakers, J. G., Langereis, C. G., & De Lange, G. J. (1993). A paleomagnetic and geochemical record of the upper Cochiti reversal and two subsequent precessional cycles from Southern Sicily (Italy). *Earth and Planetary Science Letters*, *117*(1-2), 235-250. https://doi.org/10.1016/0012-821X(93)90130-2

van Santvoort, P. J. M., de Lange, G. J., Langereis, C. G., Dekkers, M. J., & Paterne, M. (1997). Geochemical and paleomagnetic evidence for the occurrence of "missing" sapropels in eastern Mediterranean sediments. *Paleoceanography*, *12*(6), 773-786. https://doi.org/10.1029/97pa01351

Verwey, E. J. W. (1939). Electronic conduction of magnetite (Fe_3O_4) and its transition point at low temperatures. *Nature*, *144*(3642), 327-328. https://doi.org/10.1038/144327b0

Wehausen, R., & Brumsack, H. J. (2000). Chemical cycles in Pliocene sapropel-bearing and sapropel-barren eastern Mediterranean sediments. *Palaeogeography, Palaeoclimatology, Palaeoecology*, *158*(3-4), 325-352. https://doi.org/10.1016/S0031-0182(00)00057-2

Weiss, B. P., Kim, S. S., Kirschvink, J. L., Kopp, R. E., Sankaran, M., Kobayashi, A., & Komeili, A. (2004). Ferromagnetic resonance and low-temperature magnetic tests for biogenic magnetite. *Earth and Planetary Science Letters*, *224*(1-2), 73-89. https://doi.org/10.1016/j.epsl.2004.04.024

Yamazaki, T. (2008). Magnetostatic interactions in deep-sea sediments inferred from first-order reversal curve diagrams: Implications for relative paleointensity normalization. *Geochemistry, Geophysics, Geosystems*, *9*(2), Q02005. https://doi.org/10.1029/2007gc001797

Yamazaki, T., & Ikehara, M. (2012). Origin of magnetic mineral concentration variation in the Southern Ocean. *Paleoceanography*, *27*(2). https://doi.org/10.1029/2011pa002271

Yamazaki, T., & Solheid, P. (2011). Maghemite-to-magnetite reduction across the Fe-redox boundary in a sediment core from the Ontong-Java Plateau: Influence on relative palaeointensity estimation and environmental magnetic application. *Geophysical Journal International*, *185*(3), 1243-1254. https://doi.org/10.1111/j.1365-246x.2011.05021.x

Zhao, X., Heslop, D., & Roberts, A. P. (2015). A protocol for variable-resolution first-order reversal curve measurements. *Geochemistry, Geophysics, Geosystems*, *16*(5), 1364-1377. https://doi.org/10.1002/2014gc005680

Zhao, X., Roberts, A. P., Heslop, D., Paterson, G. A., Li, Y., & Li, J. (2017), Magnetic domain state diagnosis using hysteresis reversal curves, *Journal of Geophysical Research: Solid Earth*, *122*, 4767-4789. https://doi.org/10.1002/2016JB013683

Figure 1.

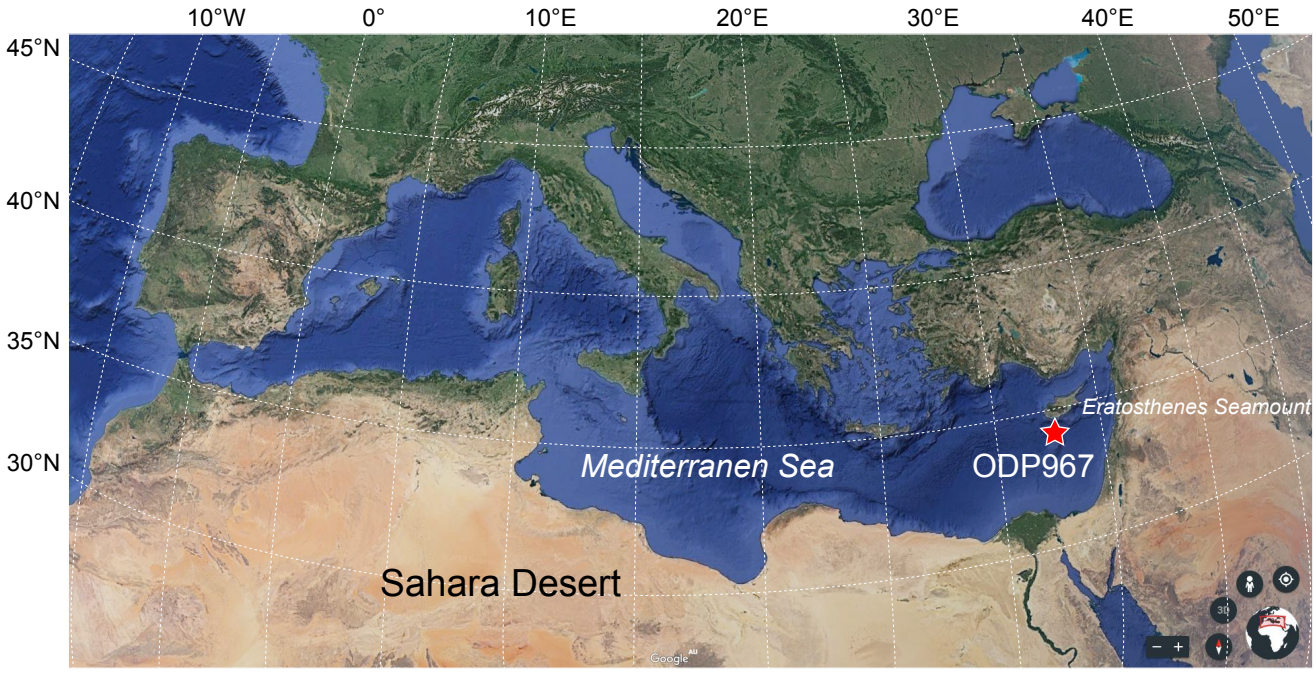
10°W
0°
10°E
20°E
30°E
40°E
50°E
45°N
40°N
35°N
30°N
Eratosthenes Seamount
Mediterranen Sea
ODP967
Sahara Desert

Figure 2.

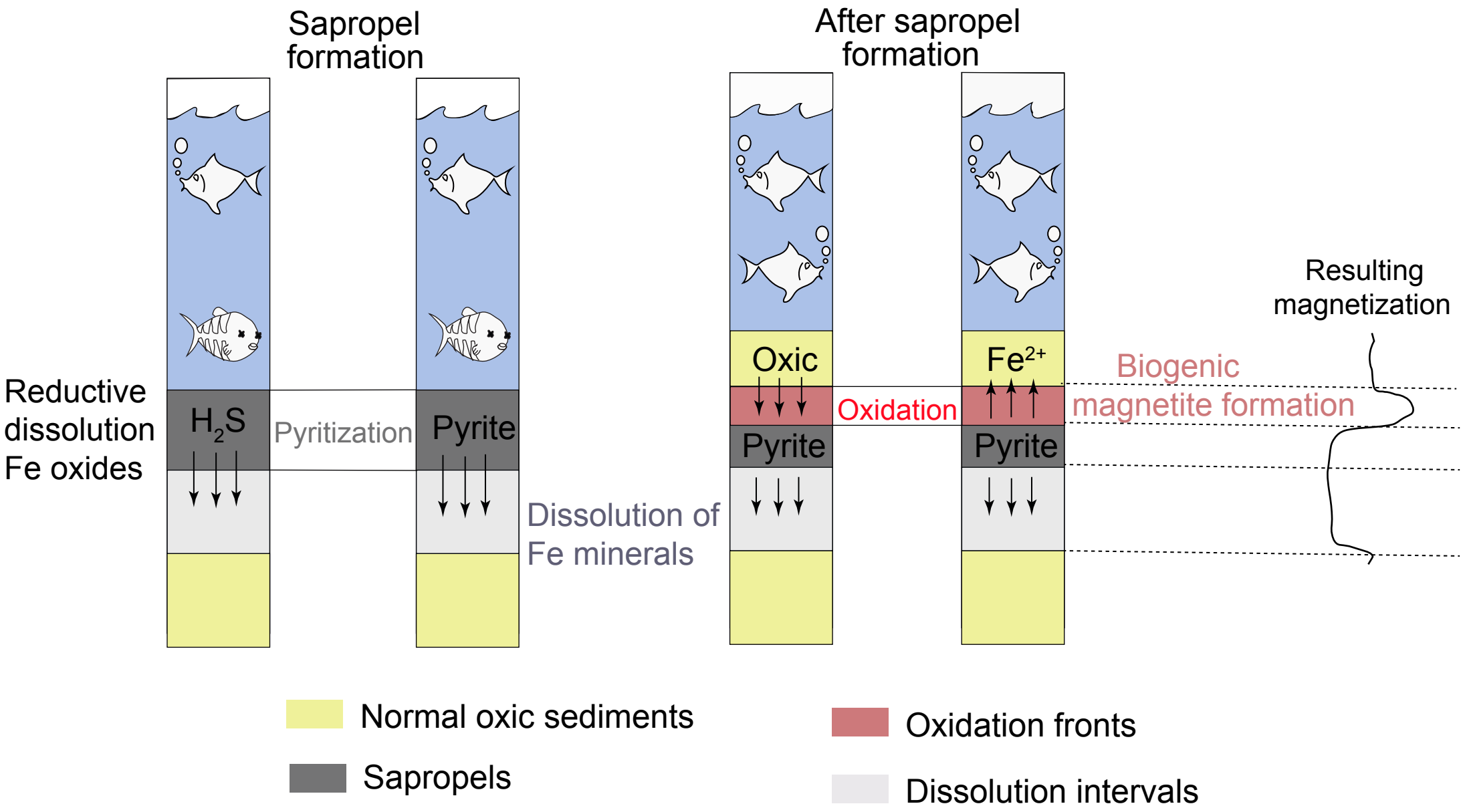
Sapropel formation
After sapropel formation
Reductive dissolution Fe oxides
H_2S
Pyritization
Pyrite
Dissolution of Fe minerals
Oxic
Fe^{2+}
Oxidation
Pyrite
Pyrite
Resulting magnetization
Biogenic magnetite formation
Normal oxic sediments
Sapropels
Oxidation fronts
Dissolution intervals

Figure 3.

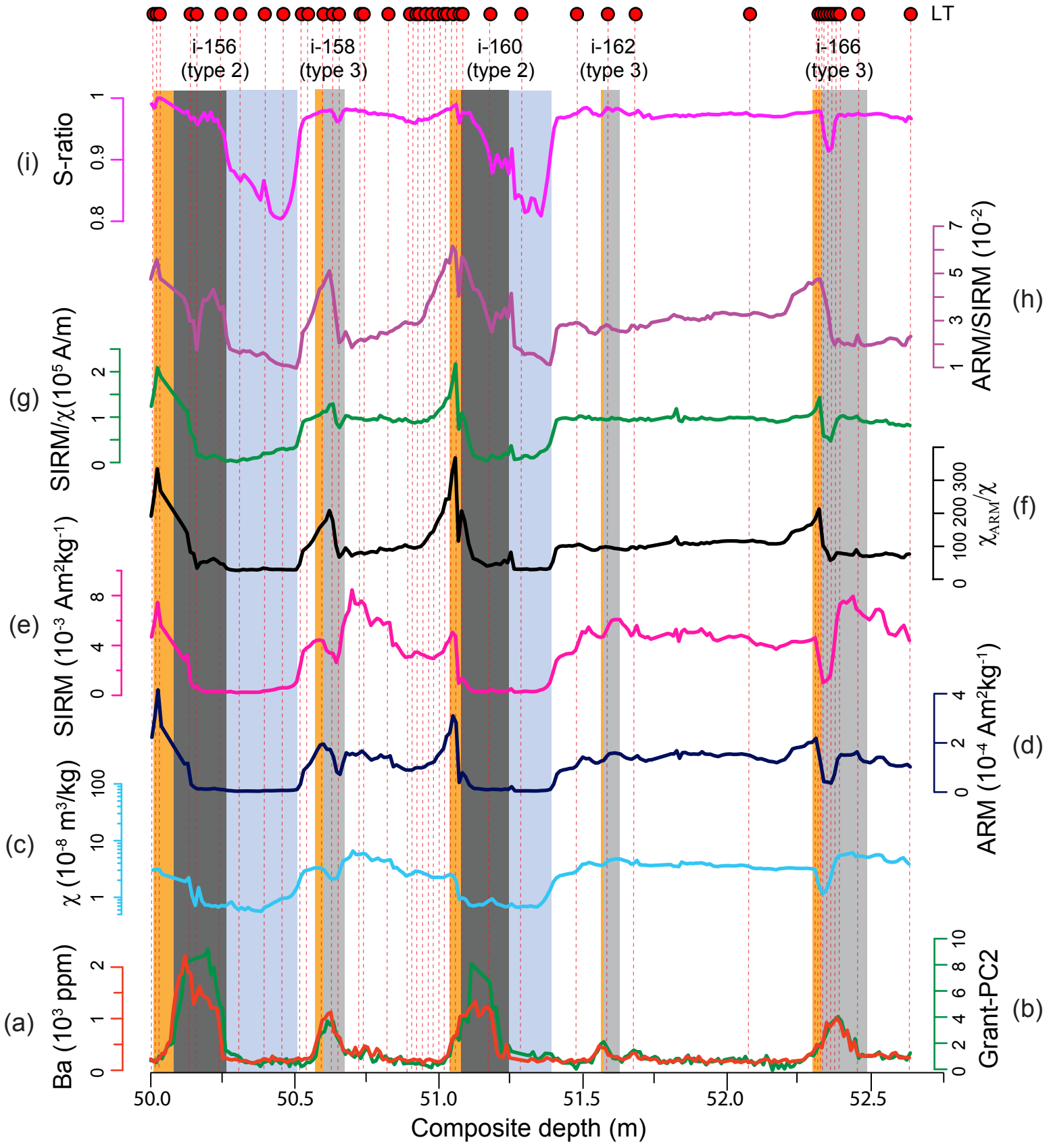
LT
i-156
(type 2)
i-158
(type 3)
i-160
(type 2)
i-162
(type 3)
i-166
(type 3)
(i)
S-ratio
0.8
0.9
1
(h)
ARM/SIRM (10-2)
1
3
5
7
(g)
SIRM/χ(10^5 A/m)
0
1
2
(f)
χARM/χ
0
100
200
300
(e)
SIRM (10-3 Am2kg-1)
0
4
8
(d)
ARM (10-4 Am2kg-1)
0
2
4
(c)
χ (10-8 m3/kg)
1
10
100
(b)
Grant-PC2
0
2
4
6
8
10
(a)
Ba (10^3 ppm)
0
1
2
50.0
50.5
51.0
51.5
52.0
52.5
Composite depth (m)
Representative sapropel
Weakly developed sapropel
Oxidation front
Dissolution interval

Figure 4.

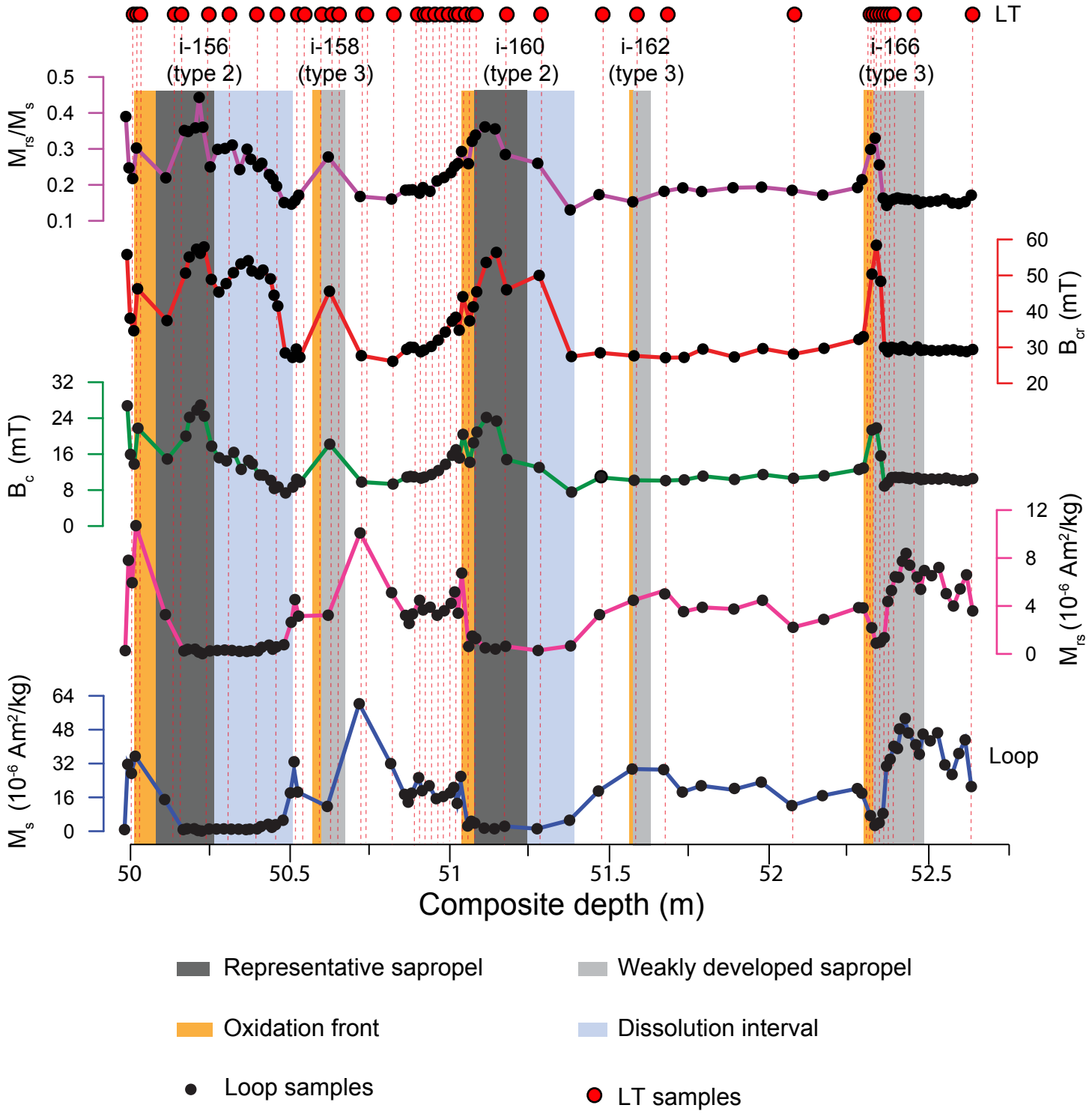
LT
i-156
(type 2)
i-158
(type 3)
i-160
(type 2)
i-162
(type 3)
i-166
(type 3)
M_{rs}/M_s
0.5
0.4
0.3
0.2
0.1
B_{cr} (mT)
60
50
40
30
20
B_c (mT)
32
24
16
8
0
M_{rs} (10^{-6} Am^2/kg)
12
8
4
0
M_s (10^{-6} Am^2/kg)
64
48
32
16
0
Loop
50
50.5
51
51.5
52
52.5
Composite depth (m)
Representative sapropel
Weakly developed sapropel
Oxidation front
Dissolution interval
Loop samples
LT samples

Figure 5.

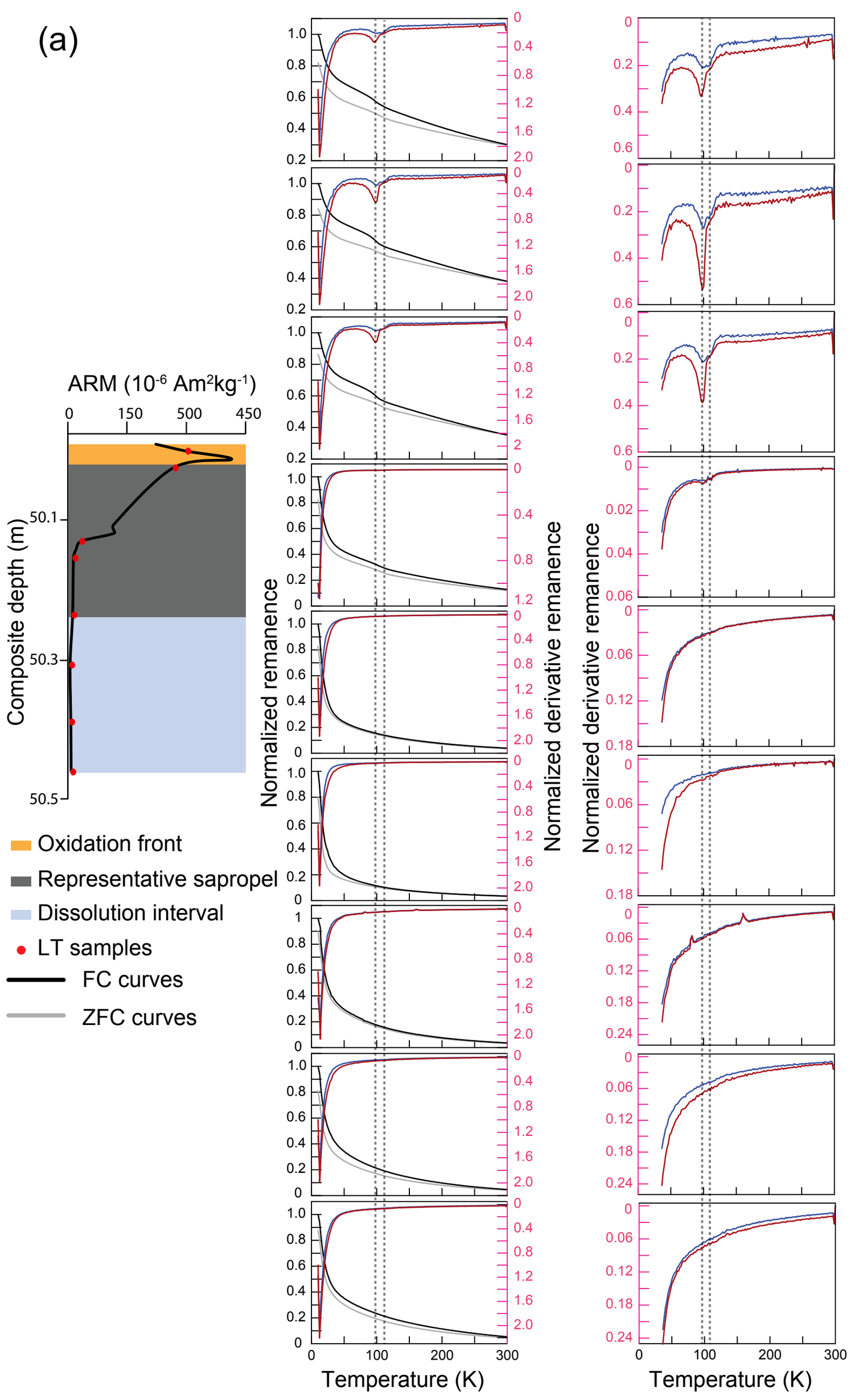
(a)
ARM (10-6 Am2kg-1)
0
150
500
450
Composite depth (m)
50.1
50.3
50.5
Oxidation front
Representative sapropel
Dissolution interval
LT samples
FC curves
ZFC curves
Normalized remanence
Normalized derivative remanence
Temperature (K)
Temperature (K)

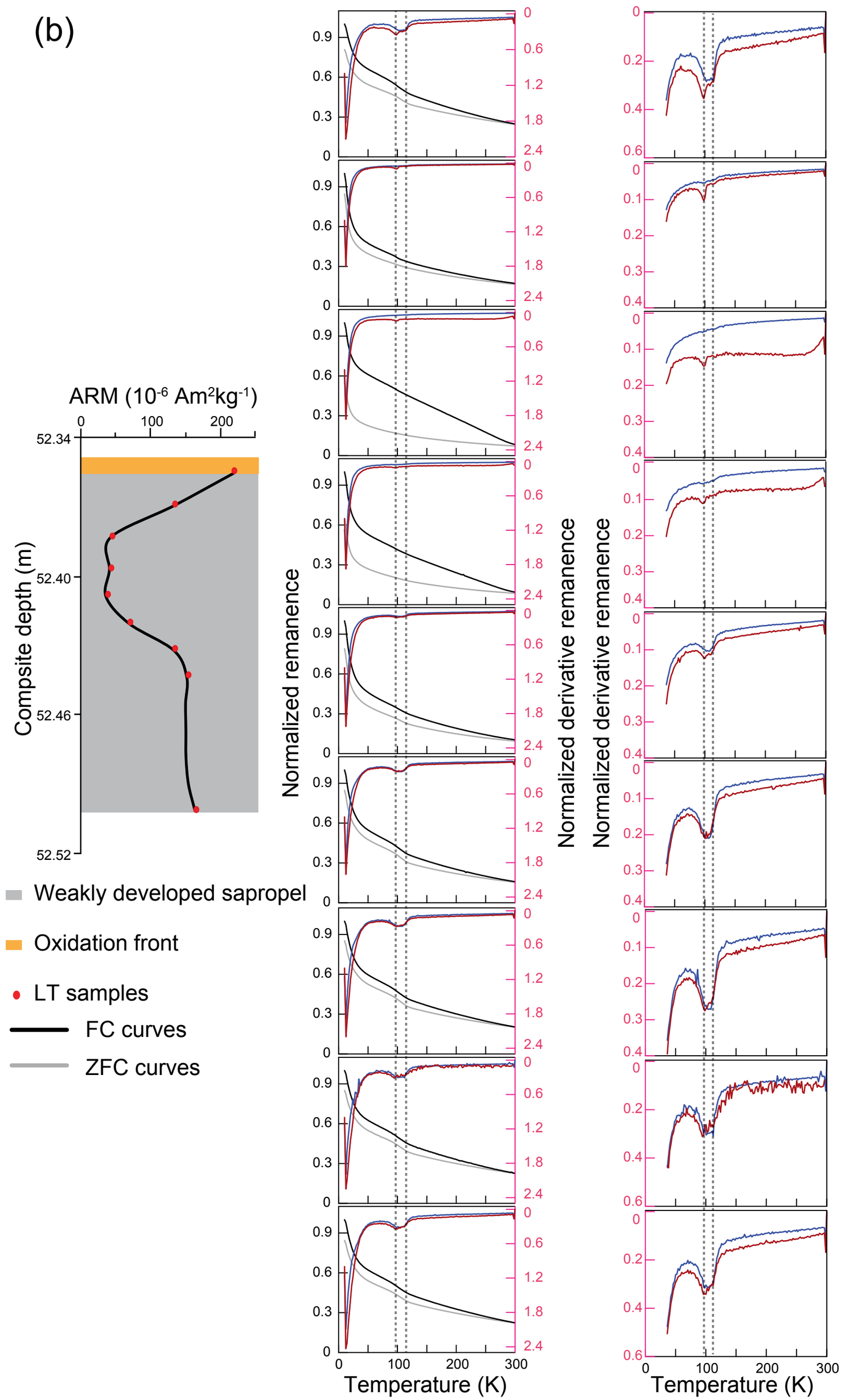
(b)
ARM (10^{-6} Am^2kg^{-1})
0
100
200
52.34
52.40
52.46
52.52
Compsite depth (m)
Weakly developed sapropel
Oxidation front
LT samples
FC curves
ZFC curves
Normalized remanence
Normalized derivative remanence
Normalized derivative remanence
Temperature (K)
Temperature (K)

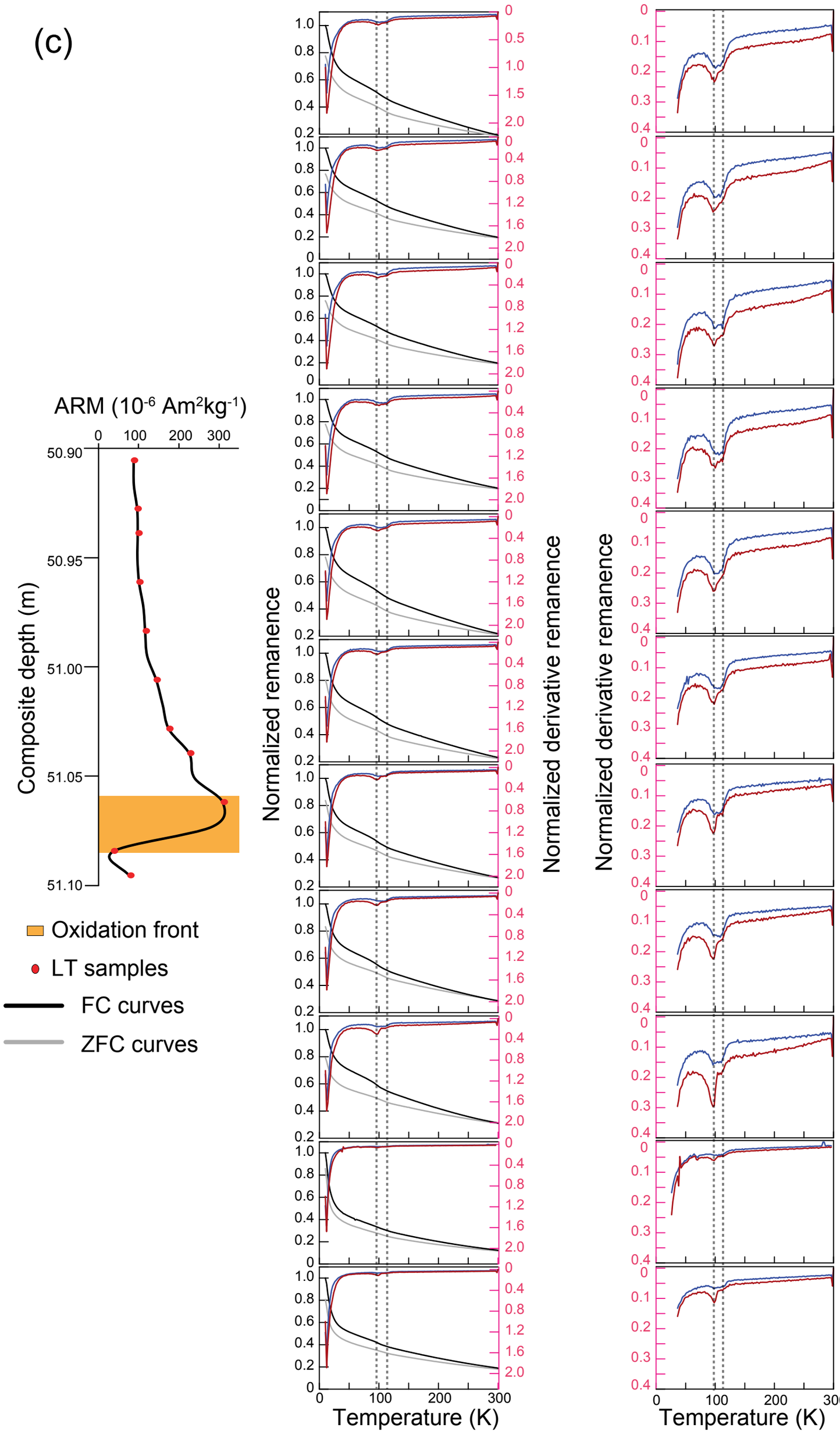
(c)
ARM (10^{-6} Am^2kg^{-1})
0
100
200
300
50.90
50.95
51.00
51.05
51.10
Composite depth (m)
Oxidation front
LT samples
FC curves
ZFC curves
Normalized remanence
Normalized derivative remanence
Normalized derivative remanence
Temperature (K)
Temperature (K)

Figure 6.

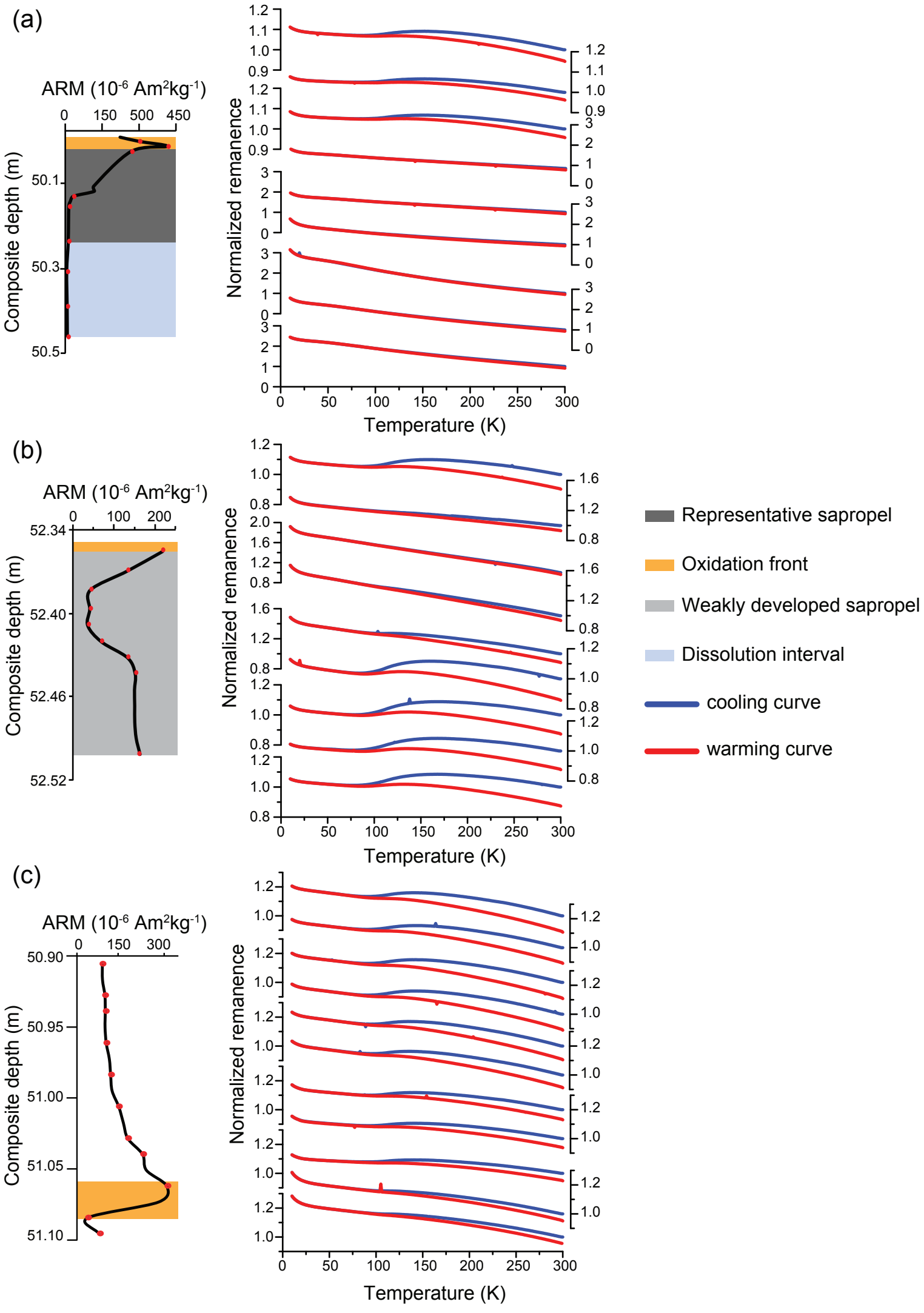
(a)
ARM (10^{-6} Am^2kg^{-1})
0 150 500 450
Composite depth (m)
50.1
50.3
50.5
Normalized remanence
Temperature (K)
(b)
ARM (10^{-6} Am^2kg^{-1})
0 100 200
52.34
52.40
52.46
52.52
Composite depth (m)
Normalized remanence
Temperature (K)
(c)
ARM (10^{-6} Am^2kg^{-1})
0 150 300
50.90
50.95
51.00
51.05
51.10
Composite depth (m)
Normalized remanence
Temperature (K)
Representative sapropel
Oxidation front
Weakly developed sapropel
Dissolution interval
cooling curve
warming curve

Figure 7.

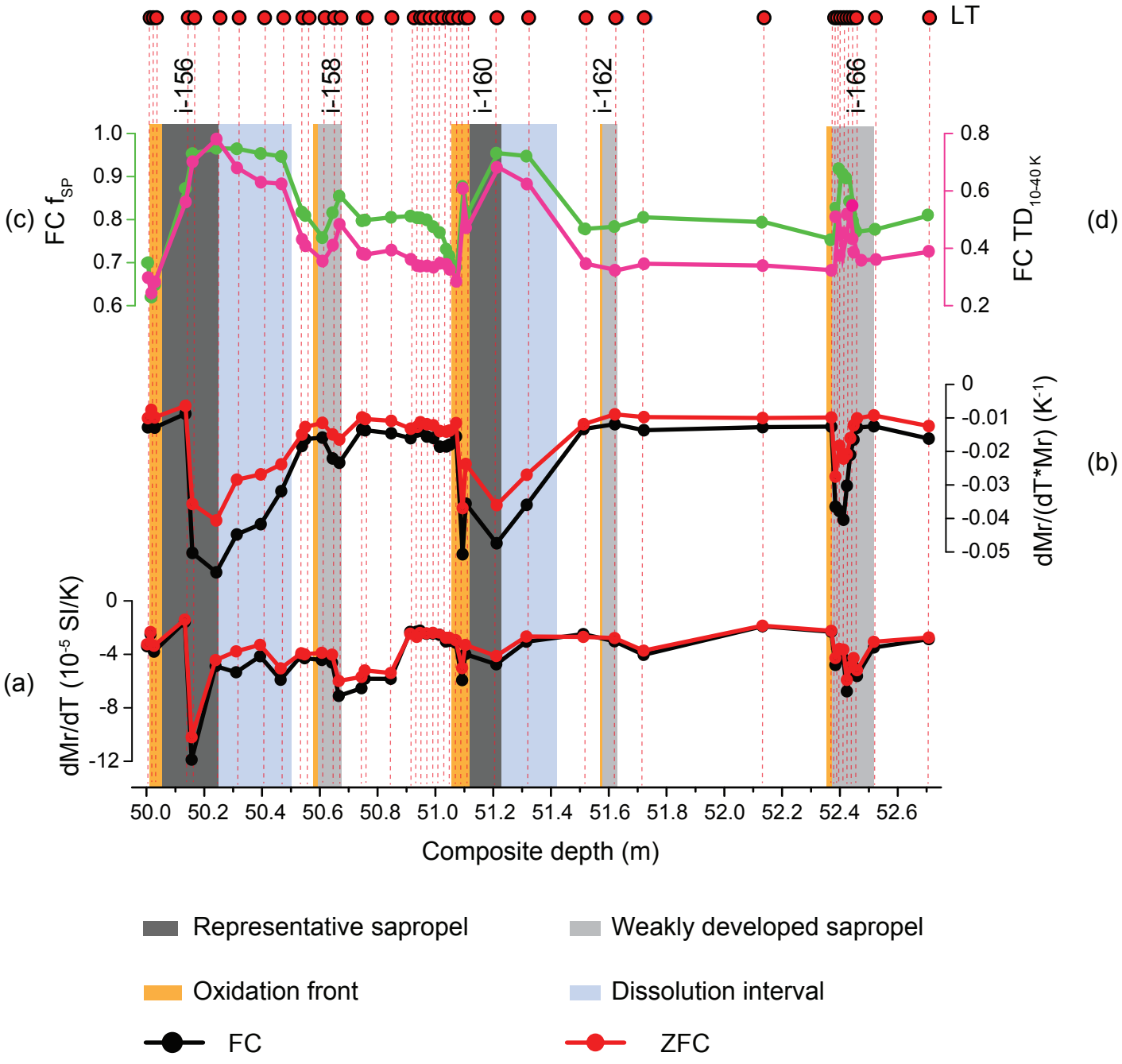
LT
i-156
i-158
i-160
i-162
i-166
(c) FC f_{SP}
1.0
0.9
0.8
0.7
0.6
FC $TD_{10\text{-}40\ K}$
(d)
0.8
0.6
0.4
0.2
dMr/(dT*Mr) (K^{-1})
(b)
0
-0.01
-0.02
-0.03
-0.04
-0.05
(a)
dMr/dT (10^{-5} SI/K)
0
-4
-8
-12
50.0
50.2
50.4
50.6
50.8
51.0
51.2
51.4
51.6
51.8
52.0
52.2
52.4
52.6
Composite depth (m)
Representative sapropel
Weakly developed sapropel
Oxidation front
Dissolution interval
FC
ZFC

Figure 8.

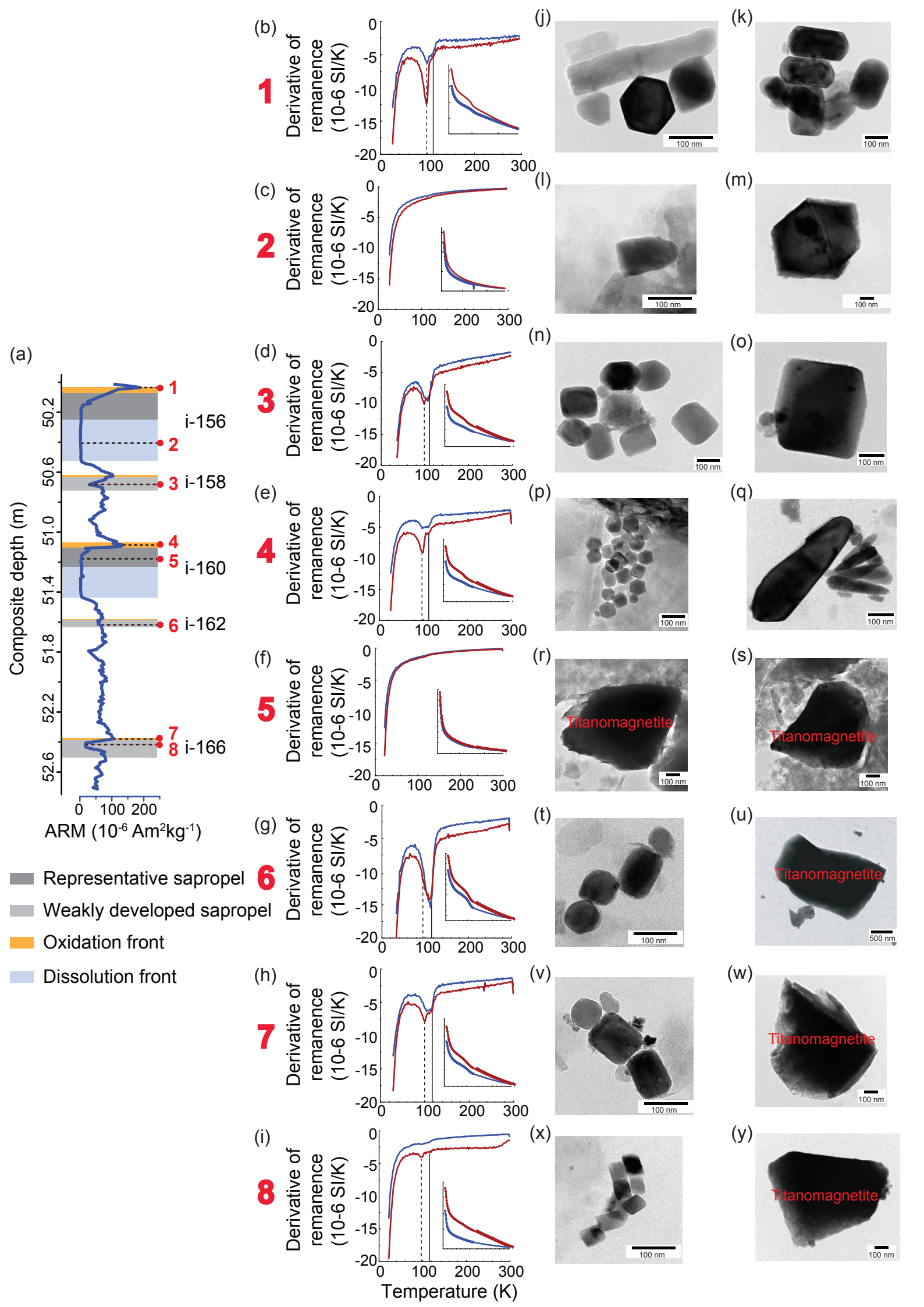
(a)
Composite depth (m)
50.2
50.6
51.0
51.4
51.8
52.2
52.6
1
2
3
4
5
6
7
8
i-156
i-158
i-160
i-162
i-166
0 100 200
ARM (10^{-6} Am^2kg^{-1})
Representative sapropel
Weakly developed sapropel
Oxidation front
Dissolution front
(b)
(c)
(d)
(e)
(f)
(g)
(h)
(i)
Derivative of remanence (10-6 SI/K)
0
-5
-10
-15
-20
0 100 200 300
Temperature (K)
(j)
(k)
(l)
(m)
(n)
(o)
(p)
(q)
(r)
(s)
(t)
(u)
(v)
(w)
(x)
(y)
100 nm
500 nm
Titanomagnetite

Figure 9.

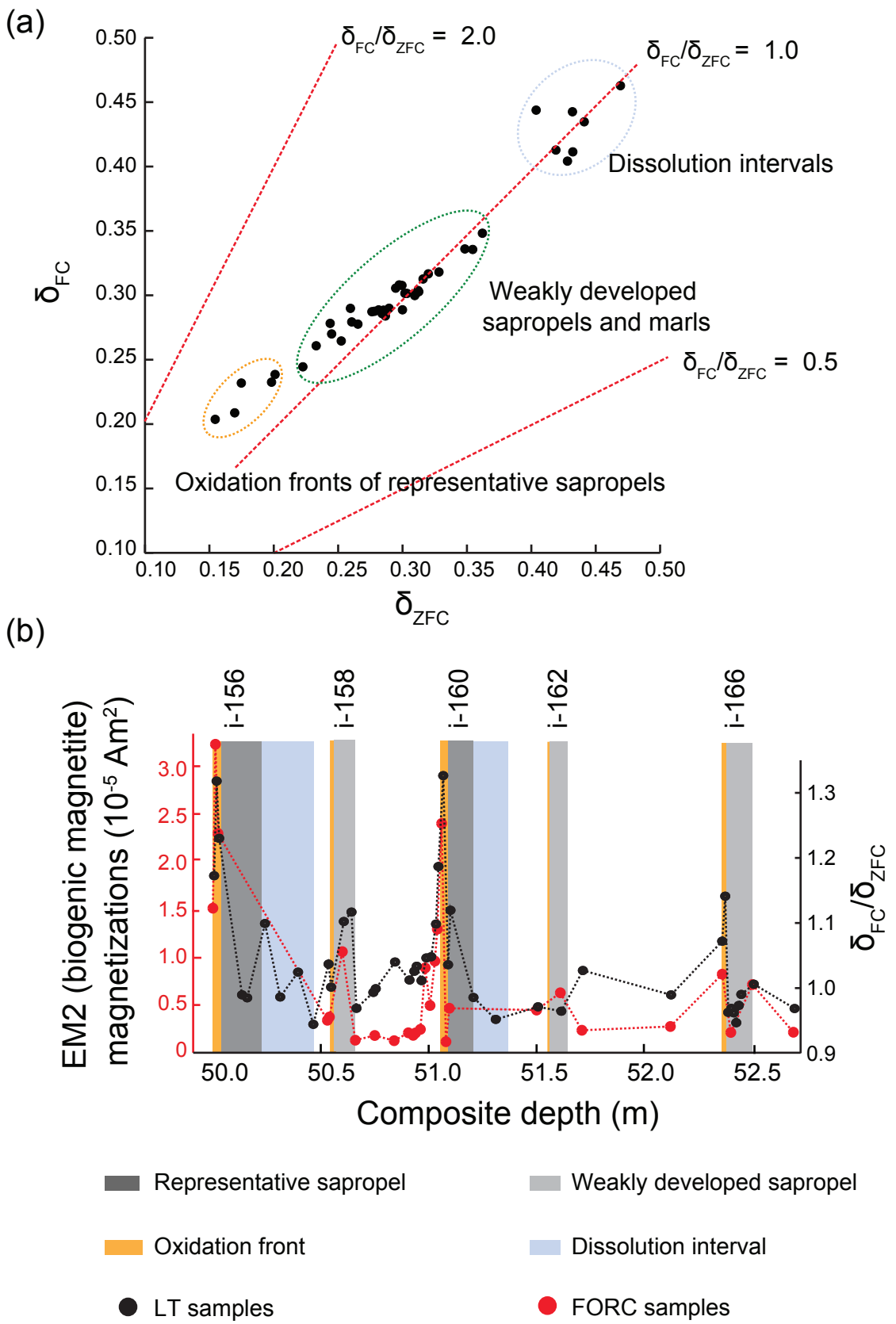
(a)
δFC/δZFC = 2.0
δFC/δZFC = 1.0
Dissolution intervals
Weakly developed
sapropels and marls
δFC/δZFC = 0.5
Oxidation fronts of representative sapropels
δFC
δZFC
0.10
0.15
0.20
0.25
0.30
0.35
0.40
0.45
0.50
(b)
i-156
i-158
i-160
i-162
i-166
EM2 (biogenic magnetite)
magnetizations (10-5 Am2)
δFC/δZFC
Composite depth (m)
50.0
50.5
51.0
51.5
52.0
52.5
Representative sapropel
Weakly developed sapropel
Oxidation front
Dissolution interval
LT samples
FORC samples

Figure 10.

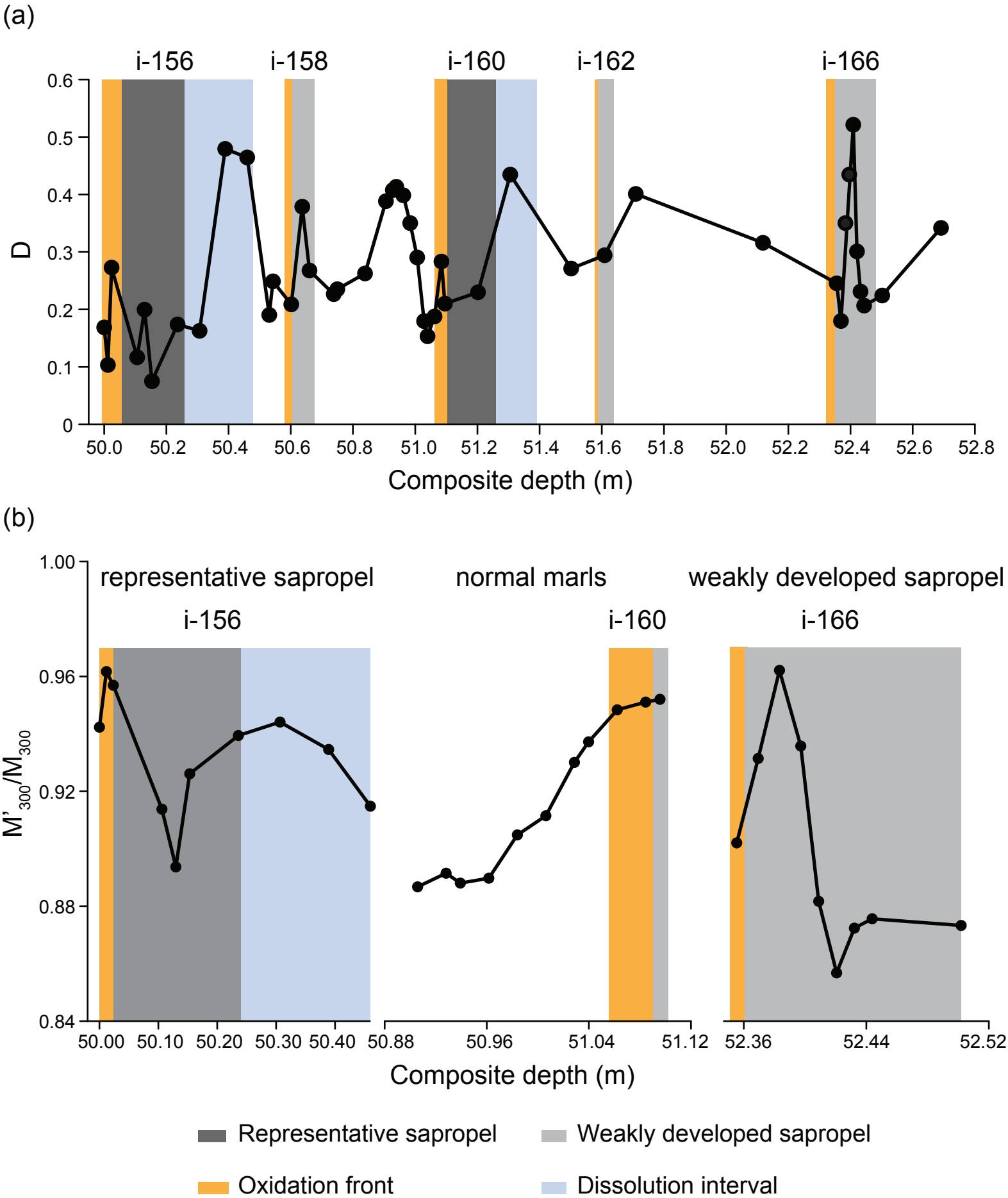
(a)
i-156
i-158
i-160
i-162
i-166
D
0.6
0.5
0.4
0.3
0.2
0.1
0
50.0
50.2
50.4
50.6
50.8
51.0
51.2
51.4
51.6
51.8
52.0
52.2
52.4
52.6
52.8
Composite depth (m)
(b)
representative sapropel
normal marls
weakly developed sapropel
i-156
i-160
i-166
M'300/M300
1.00
0.96
0.92
0.88
0.84
50.00
50.10
50.20
50.30
50.40
50.88
50.96
51.04
51.12
52.36
52.44
52.52
Composite depth (m)
Representative sapropel
Weakly developed sapropel
Oxidation front
Dissolution interval